IEEE Access
Multidisciplinary | Rapid Review | Open Access Journal

Received 21 July 2023, accepted 3 September 2023, date of publication 19 September 2023, date of current version 6 October 2023.

Digital Object Identifier 10.1109/ACCESS.2023.3317241

RESEARCH ARTICLE

A Hybrid Compressive Sensing and Classification Approach for Dynamic Storage Management of Vital Biomedical Signals

HEBA M. EMARA[1], WALID EL-SHAFAI[2,3], (Senior Member, IEEE), ABEER D. ALGARNI[4], NAGLAA F. SOLIMAN[4], AND FATHI E. ABD EL-SAMIE[4]

[1]Department of Electronics and Communications Engineering, Pyramids High Institute of Electronic Engineering, Ministry of Higher Education, 6th of October, Giza 2591, Egypt
[2]Security Engineering Laboratory, Computer Science Department, Prince Sultan University, Riyadh 11586, Saudi Arabia
[3]Department of Electronics and Electrical Communications Engineering, Faculty of Electronic Engineering, Menoufia University, Menouf 32952, Egypt
[4]Department of Information Technology, College of Computer and Information Sciences, Princess Nourah Bint Abdulrahman University, Riyadh 11671, Saudi Arabia

Corresponding authors: Heba M. Emara (heba.emara@el-eng.menofia.edu.eg) and Abeer D. Algarni (adalqarni@pnu.edu.sa)

This work was supported by the Deputyship for Research & Innovation, Ministry of Education, Saudi Arabia, under Project RI-44-0528.

ABSTRACT The efficient compression and classification of medical signals, particularly electroencephalography (EEG) and electrocardiography (ECG) signals in wireless body area network (WBAN) systems, are crucial for real-time monitoring and diagnosis. This paper addresses the challenges of compressive sensing and classification in WBAN systems for EEG and ECG signals. To tackle the challenges of the compression process, a sequential approach is proposed. The first step involves compressing the EEG and ECG signals using the optimized Walsh-Hadamard transform (OWHT). This transform allows for efficient representation of the signals, while preserving their essential characteristics. However, the presence of noise can impact the quality of the compressed signals. To mitigate this effect, the signals are subsequently recovered using the Sparse Group Lasso 1 (SPGL1) algorithm and OWHT, which take into account the noise characteristics during the recovery process. To evaluate the performance of the proposed compressive sensing algorithm, two metrics are employed: mean squared error (MSE) and maximum correntropy criterion (MCC). These metrics provide insights into the accuracy and reliability of the recovered signals at different signal-to-sample ratios (SSRs). The results of the evaluation demonstrate the effectiveness of the proposed algorithm in accurately reconstructing the EEG and ECG signals, while effectively managing the noise interference. Furthermore, to enhance the classification accuracy in the presence of signal compression, a local binary pattern (LBP) tehnique is applied. This technique extracts discriminative features from the compressed signals. These features are then fed into a classification algorithm based on residual learning. This classification algorithm is trained from scratch and specifically designed to work with the compressed signals. The experimental results showcase the high accuracy achieved by the proposed approach in classifying the compressed EEG and ECG signals without the need for signal recovery. The findings of this study highlight the potential of the proposed approach in achieving efficient and accurate medical signal analysis in WBAN systems. By eliminating the computational burden of signal recovery and leveraging the advantages of compressive sensing, the proposed approach offers a promising solution for real-time monitoring and diagnosis, ultimately improving the overall efficiency and effectiveness of healthcare systems.

INDEX TERMS Compressive sensing, EEG, ECG, OWHT, LBP, classification, SPGL1, WBAN, deep learning.

I. INTRODUCTION

In recent years, the increasing popularity of smart homes has been driven by advancements in artificial intelligence and

The associate editor coordinating the review of this manuscript and approving it for publication was Hasan S. Mir.

Internet of Things (IoT), which enhance the quality of living for individuals [1], [2]. Among the key aspects of smart home applications are indoor localization, activity recognition, and healthcare monitoring. WiFi-based sensing systems are utilized for indoor localization and human activity recognition, while wireless body area networks (WBANs) are employed for continuous and real-time monitoring of healthcare parameters [3]. WBANs are particularly effective in monitoring of cardiovascular health through the use of electrocardiographs (ECGs), allowing for early detection of underlying cardiovascular diseases [4]. ECG signals are acquired through wearable devices and wirelessly transmitted to the system back-end for storage and further analysis. However, one critical challenge is the energy consumption of the sensors, which impacts the lifetime and portability of wearable devices. They have limited battery capacities, imposing constraints on sampling techniques, and traditional solutions based on Nyquist-Shannon theory are inadequate for signal acquisition in wearable sensors [5]. WBANs offer the potential for remote monitoring of biomedical signals, such as EEG and ECG signals [6], [7].

Compressive sensing offers a promising solution for continuous ECG signal monitoring using wearable devices [8]. By leveraging the sparsity of signals in specific domains, compressive sensing allows a simple linear sampling process to acquire signals, which are then reconstructed. This approach significantly reduces the complexity of data encoding, fulfills the requirements of data transmission and storage, and proves to be highly suitable for WBAN applications [9], [10]. The effectiveness of compressive sensing has been demonstrated in various fields, including IoT applications [11], [12], [13]. It has the potential to greatly extend the monitoring lifespan of bio-sensors. In the context of ECG monitoring with wearable devices, previous researchers have explored the application of compressive sensing. Specifically, adaptive overcomplete dictionaries can be selected based on the QRS estimation of compressed measurements in each frame, leading to improved reconstruction quality of ECG signals [14]. This adaptive approach enhances the accuracy and reliability of ECG signal monitoring, enabling more effective healthcare monitoring in WBAN systems.

The application of compressive sensing has demonstrated its potential to extend the monitoring lifespan of biosensors and meet clinical requirements in healthcare settings. However, there are certain limitations associated with the utilization of compressive sensing for ECG signal monitoring. One limitation is the potential impact of noise and interference on the quality of reconstructed ECG signals. The presence of noise can degrade the accuracy and reliability of signal interpretation and analysis. Additionally, selecting an appropriate dictionary for each frame can be a challenging task that requires further optimization. Moreover, compressive sensing may not be suitable for all types of ECG monitoring applications, as it may not capture certain signal features that are essential for specific diagnostic purposes. The acquisition and analysis of ECG signals play a crucial role in diagnosing and monitoring of various cardiac conditions. However, ECG signals often suffer from contamination by different types of noise, which can hinder accurate interpretation and analysis [15]. Muscle artifacts and power line interference are two common sources of noise in ECG signals. Muscle artifacts arise from the contraction of nearby muscles, generating unwanted electrical activities that obscure the underlying cardiac signal [16]. These artifacts appear as high-frequency noise or spikes superimposed on the ECG waveform, posing challenges in detecting important features. On the other hand, power line interference, also known as mains interference, occurs due to the presence of alternating-current (AC) power lines. This interference introduces regular and repetitive waveforms synchronized with the mains frequency, typically 50 Hz or 60 Hz. Power line interference manifests itself as periodic spikes or oscillations superimposed on the ECG signal. It can obscure the desired cardiac activity. Understanding and addressing these sources of noise are critical for obtaining reliable and accurate ECG measurements, enabling more precise diagnosis and monitoring of cardiac conditions. Various techniques, such as signal processing algorithms and proper electrode placement, can be employed to mitigate these noise sources and enhance the quality of ECG recordings [17].

In recent years, there has been a growing interest in leveraging deep learning techniques for the classification and diagnosis of various diseases based on biomedical signals and images [18], [19], [20], [21], [22], [23], [24], [25]. Specifically, deep learning models, including Convolutional Neural Networks (CNNs) and Recurrent Neural Networks (RNNs), have shown tremendous potential in analyzing Electroencephalogram (EEG) signals and extracting meaningful features for disease classification. These models possess the capability to automatically learn complex patterns and relationships within the EEG data, enabling accurate and efficient diagnosis of conditions such as epilepsy, sleep disorders, and neurodegenerative diseases. The application of deep learning in EEG signal classification offers several advantages. Firstly, deep learning models demonstrate high accuracy in detecting and classifying neurological conditions. They have been trained on large datasets, allowing them to generalize well to unseen samples and provide reliable predictions. Moreover, deep learning models are robust to noise and artifacts commonly present in EEG signals, making them suitable for real-world applications. Their ability to handle noisy data enhances the overall performance and ensures accurate disease diagnosis. Additionally, deep-learning-based analysis of EEG signals has the potential for real-time processing, enabling prompt medical intervention and continuous monitoring of patients.

The integration of deep learning models into EEG classification has the potential to revolutionize the field of neurology and significantly improve patient care. By enabling early detection of neurological disorders, personalized treatment

plans can be devised, leading to improved outcomes and a higher quality of life for patients. However, there are still challenges to overcome in this domain. One of the key challenges is the availability of large and diverse datasets for training of deep learning models. Access to well-annotated EEG datasets is crucial to ensure optimal model performance and generalizability across different patient populations. Additionally, interpretability of deep learning models remains an area of active research.

The utilization of EEG signals for monitoring of brain activities and diagnosis of epilepsy offers a non-invasive approach. However, the manual process of seizure detection in long-duration EEG recordings is time-consuming for medical professionals. To expedite this process and enable real-time seizure detection, automated systems are desired. Implementing such systems would alleviate the burden of visually scoring extensive EEG records, thereby providing faster identification of seizures [26].

Wireless seizure detection systems based on EEG signals can adopt different approaches, each with its own set of advantages and limitations. One of these approaches involves transmitting the entire raw EEG data to a remote terminal and utilizing various algorithms, such as deep learning, filter bank, empirical mode decomposition, and entropy analysis, which have been explored in the literature for accurate seizure detection [27], [28], [29]. Another recent approach, utilizing the Matrix Determinant (MD) of EEG signals as a feature, has demonstrated excellent seizure detection performance with low execution time [30]. However, it is important to note that transmitting the raw EEG data comes with certain drawbacks. It requires high energy consumption at the sensor node and demands a large bandwidth, making it unsuitable for implementation in WBAN systems. These limitations pose challenges for deploying wireless seizure detection systems that aim for low-power consumption and efficient use of limited resources in WBANs. New strategies are needed to overcome these limitations and develop energy-efficient and bandwidth-friendly solutions for real-time seizure detection in wireless EEG-based systems.

An alternative approach to wireless seizure detection systems is the extraction of relevant features from the raw EEG data at the sensor node, which are then transmitted to a remote terminal for classification. This approach offers the advantage of conserving energy in data encoding and transmission. However, it has been observed to have lower effectiveness in detecting seizures compared to other methods. One limitation of this approach is the need to select simple features with low computational requirements at the sensor node. This is necessary to minimize power consumption and extend battery life of sensors. Complex feature extraction tends to consume more power, which may significantly reduce the lifespan of the sensor batteries [31]. Therefore, careful consideration and optimization of feature selection are essential to strike a balance between energy efficiency and seizure detection performance in wireless EEG-based systems.

An alternative approach for wireless EEG-based seizure detection systems is the use of compressive sensing techniques to efficiently compress the EEG data before transmission. Traditional compression methods, such as Set Partitioning In Hierarchical Trees, are not suitable for WBAN systems due to their high complexity and computational requirements. Compressive sensing offers a more efficient approach by reducing both processing load and transmission energy in WBANs. Previous studies have demonstrated the effectiveness of compressive sensing in classifying EEG signals for seizure detection. Altered EEG compressibility, quantified by metrics such as Normalized Mean Squared Error (NMSE) and structural similarity (SSIM), has been used as a feature for distinguishing seizure-free, pre-seizure, and seizure states. Results have shown that compressive-sensing-based NMSE and SSIM outperform other metrics, such as sample entropy and permutation entropy, in epileptic seizure classification, making them valuable biomarkers for diagnosing seizure states [32]. When designing a WBAN-based EEG monitoring system for seizure detection, two primary constraints need to be considered: energy consumption and processing time. Compressive sensing techniques can help conserve energy during EEG sensing and transmission. However, existing seizure detection methods often require full reconstruction of the original EEG signals from the compressed data, which is time-consuming and computationally intensive. To enable real-time applications in WBANs, there is a need to develop fast and efficient automatic seizure detection methods that can operate directly on the compressed signals without the need for full reconstruction.

However, it is worth noting that the existing literature on seizure detection in compressive-sensing-based WBAN systems primarily focuses on the recovery of the full original EEG samples at the remote terminal. The computational complexity involved in achieving high-quality signal recovery poses limitations on the practicality of these methods for real-time disease detection. To address these challenges and enable real-time diagnosis of brain disorders using dense neural sensor data, advanced signal processing approaches are required. Compressive sensing offers an efficient solution for reducing computational complexity and power consumption. However, the signal reconstruction phase can still be computationally intensive, hindering real-time applications such as seizure detection. In this study, a sequential approach is proposed to overcome the limitations of traditional compressive sensing methods in WBAN systems for EEG and ECG signals. The proposed approach aims to efficiently compress and classify the medical signals without the need for full signal recovery. By utilizing the OWHT for compression and the SPGL1 algorithm for signal recovery, while considering the presence of noise, the proposed approach achieves accurate reconstruction of signals. Moreover, the application of the LBP technique and a classification algorithm based on residual learning further enhances the classification accuracy with compressed

signals. This approach enables efficient compression, reliable signal recovery, and accurate classification, facilitating real-time disease detection in WBAN systems. By leveraging the benefits of compressive sensing, while addressing the computational challenges associated with signal recovery, the proposed sequential approach provides a promising solution for efficient and accurate diagnosis of brain disorders using compressed signals.

The main contributions of this paper can be summarized as follows:

- The proposed sequential approach combines compressive sensing and classification techniques to address the challenges of medical signal analysis in WBAN systems.
- The use of the OWHT for compression and the SPGL1 algorithm for signal recovery allows for efficient reconstruction of EEG and ECG signals, while considering the impact of noise.
- The application of the LBP technique and a classification algorithm based on residual learning enhances the classification capabilities with compressed signals.
- The proposed algorithm enables real-time monitoring and diagnosis without the need for signal recovery, reducing computational burden and improving the efficiency of healthcare systems.

The subsequent sections of this paper are structured as follows. In Section II, a thorough review of existing literature pertaining to medical signal analysis in WBAN systems is presented, focusing on the limitations and gaps observed in current approaches. Section III outlines the proposed methodology, along with details regarding the experimental setup and evaluation metrics employed to assess the performance of the proposed approach. The results and analysis derived from the conducted experiments are presented in Section IV. They are followed by a comprehensive discussion of the findings and implications. Finally, Section V introduces the paper conclusion by summarizing the contributions of this study and giving potential avenues for future research.

II. RELATED WORK

Recently, there has been a growing interest in using compressive sensing for compressing ECG data. Traditional recovery methods based on sparse optimization with priors face challenges. Unni et al. [33] introduced Plug-and-Play (PnP), an iterative recovery algorithm with a powerful denoiser that incorporates regularization. The PnP version of Proximal Gradient Descent (PGD) depends on a denoiser trained with a Bayesian prior for small-size signal patches. Giovanni et al. [34] presented enhanced NEAPOLIS, an approach for real-time arrhythmia detection, for analyzing compressed ECG signals. They refined and optimized NEAPOLIS features to align with the compression algorithm. Extensive investigation was introduced to evaluated the classification performance at different compression ratios. Results showed that the updated NEAPOLIS effectively operates with highly compressed ECG signals, achieving a compression ratio of 16.

Compressive sensing is widely used for compressing ECG data in resource-constrained wearable devices. Kumar et al. introduced a codec architecture that incorporates adaptive quantization and Asymmetric Numeral Systems (ANS) for efficient compression [35]. The approach dynamically adapts a quantized Gaussian entropy model to improve compression performance, achieving additional space savings compared to conventional techniques. Fira et al. analyzed the trade-off between preprocessing complexity and reconstruction accuracy in compressive sensing for ECG signals [36]. They proposed application-specific dictionaries and tested them with various projection matrices. Quantitative and qualitative evaluations demonstrated the quality of the reconstructed signals using standard distortion measures and classification techniques. Aghazadeh et al. presented a seizure detection algorithm that directly processes compressively-sampled EEG signals, bypassing reconstruction [37]. They utilized spectral energy features and a non-linear SVM classifier for high-performance seizure detection. They also proposed a power-efficient classification those of method and demonstrated a hardware-optimized implementation achieving high accuracy with a low energy budget.

Compressive sensing techniques are employed in ECG monitoring to reduce data and energy costs. Hua et al. [38] proposed a deep compressive sensing framework using a modified Inception block and LSTM, achieving improved reconstruction performance across various sensing rates. Their method demonstrated the lowest Percentage Root-mean-square Difference (PRD) and the highest Signal-to-Noise Ratio (SNR) compared to those of other methods, with the PRD dropping below 2% at sensing rates exceeding 0.5. Lee et al. [39] develop an efficient deep learning method with model compression for arrhythmia classification in an embedded wearable device. Comparing Resnets and Mobilenets, both models show high accuracy, with Resnet-50 Hz achieving 97.3% and Mobilenet-50 Hz achieving 97.2% accuracy. The compressed models significantly reduce weight size from 743 MB to 76 KB, without substantial loss in performance. Abdelazez et al. [40] proposed a Signal Quality Index (SQI) for evaluating compressively-sensed ECG signals. The SQI, based on random forests, exhibits good performance across different databases and compression ratios. The average RMSE values for normal and abnormal ECG signals are 3.18 dB and 3.47 dB, respectively. The average Spearman correlation values reach 94% for normal ECG and 93% for abnormal ECG. The SQI achieves an average accuracy of 90% and an F1 score of 88%.

Remote ECG monitoring is essential for cardiovascular health, but it faces challenges due to data volume and device limitations. Compressive sensing provides a solution, but traditional algorithms are time-consuming. Zhang et al. proposed a fast reconstruction algorithm using compressive sensing and deep learning [41]. It combines CNN and LSTM to directly learn the mapping relationship between measure-

ments and original ECG signals. Experimental results on the MIT-BIH Arrhythmia Database show superior performance compared to traditional algorithms such as BP, OMP, BSBL-BO, and R-SVD+BP [41]. The proposed method achieves significantly faster reconstruction, requiring only 0.12 seconds for a 30-minute ECG signal, and outperforms traditional algorithms even at high compression ratios of up to 90%.

ECG classification plays a crucial role in diagnosing cardiovascular conditions. Various methods, including traditional machine learning and deep learning ones, have been utilized [42], [43], [44], [45], [46], [47], [48], [49]. These methods involve feature extraction and classification models to categorize ECG signals, accurately. They have shown promising results in achieving high accuracy for early detection and intervention [50], [51], [52], [53], [54]. Ongoing research focuses on enhancing feature extraction, optimizing classification models, and integrating multi-modal data. Effective ECG classification systems hold great potential for improving cardiovascular healthcare and patient care.

In the domain of mobile epileptic seizure treatment, Qaisar et al. [55] proposed an adaptive rate processing-based method for efficient and automated epilepsy detection. By dynamically adjusting the processing rate based on EEG signal characteristics, the method significantly achieves better compression and processing efficiency compared to those of fixed-rate approaches. Compressive sensing offers a solution for EEG signal compression. Rani et al. [56] utilized compressive sensing for EEG signal acquisition and reconstruction, achieving high accuracy in epileptic seizure detection. Zhang et al. [6] introduced Block Sparse Bayesian Learning (BSBL) for telemonitoring EEG signals, outperforming existing compressed sensing algorithms in recovery quality. Liu et al. [57] proposed the Simultaneous Cosparsity and Low-Rank (SCLR) approach to enhance the efficiency and accuracy of compressed-sensing-based EEG signal processing. In the context of smart grids, Tan et al. [58] investigated the joint design of data compression and Medium Access Control (MAC) protocols using compressed sensing techniques. Their framework improves the efficiency and performance of data compression and MAC protocols in smart grid applications with renewable energy sources. Wan et al. [59] presented a Robust Bayesian Compressed Sensing (RBCS) method that effectively handles outliers in signal recovery. These advancements in adaptive rate processing, compressive sensing, and robust signal recovery contribute to improved healthcare systems, smart grids, and telemonitoring applications.

Aghababaei et al. [26] proposed a real-time automatic seizure detection method for compressed EEG data in WBANs. The method introduced the Partial Energy Difference (PED) feature, enabling seizure detection without full signal reconstruction. The results demonstrated the effectiveness of the PED feature in classifying seizure and non-seizure states, even at low compression ratios of 0.05. The single-channel method achieved up to a 4% improvement in the area under the curve, and the multivariate feature achieved high mean AUC values of 94.1%. Li et al. [60] introduced the Sparse and Low-Rank Representation in the presence of Mixed Noise (SLRMN) method for robust multichannel EEG signal compression. The SLRMN method improved the curacy of compressed signal recovery in the presence of mixed noise. Rani et al. [61] proposed a Compressed Signal Processing (CSP) method for epileptic seizure detection in EEG signals. The CSP method allows effective seizure detection without the need for full signal reconstruction. Kunabeva et al. [62] introduced an algorithm for improved analysis of epileptic disorders using an optimal mother wavelet and block adaptive decomposition. The algorithm achieved excellent reconstruction quality with low average PRD values, indicating its suitability for biomedical analysis in the detection of epileptic disorders using recovered EEG signals.

Sheykhivand et al. [63] proposed an automated system for driver fatigue detection using compressive sensing and deep neural networks based on EEG signals. The system achieved high accuracies ranging from 92% to 95% for different compression rates, demonstrating its effectiveness in detecting driver fatigue. Van et al. [64] presented EffiCSense, a framework for efficient pathfinding of mixed-signal sensor front-ends in regular and compressive sensing systems. The framework accelerated the design process by utilizing high-level functional models and power consumption models. Simulations usage of EEG signal processing for epilepsy detection showed that an optimized design with compression can be up to 3.6 times more power-efficient, while maintaining high detection accuracy. In the field of epileptic seizure detection, various techniques have been developed for automatic seizure detection using statistical features extracted from multi-channel EEG data [65], [66], [67], [68], [69], [70]. Hardware implementations in wearable EEG devices have also been explored for real-time seizure detection [71]. The continuous efforts in this field aim to improve accuracy and efficiency for effective patient care and management, including patient-specific algorithms and alternative data transformation techniques. Overall, the advancements in driver fatigue detection, efficient pathfinding, and epileptic seizure detection highlight the ongoing progress in developing reliable and efficient algorithms for detecting abnormal brain activity and improving healthcare outcomes.

III. MATERIALS AND METHODS

A. DATASET DESCRIPTION

The CHB-MIT dataset [72] was jointly developed by Children's Hospital Boston and the Massachusetts Institute of Technology (MIT). It provides noninvasive EEG recordings from 23 pediatric patients, including male patients aged between 3 and 22 years and female patients aged between 1.5 and 19 years. The EEG signals were recorded using the International 10–20 system, with a sampling rate of 256 Hz and 16-bit resolution. Each 1600-second EEG signal was

segmented into 1600 non-overlapping blocks of length $N = 256$. This resulted in EEG data matrices $X_l \in \mathbb{R}^{N \times R}$ for $l = 1, 2, \ldots, L$. Each segment of the EEG data matrix had $N \times R = 256 \times 23$ sampling points.

The ECG data used in this study were obtained from three distinct groups or classes of people: those with cardiac arrhythmia (ARR), congestive heart failure (CHF), and normal sinus rhythms (NSR). A total of 162 ECG recordings were utilized from three PhysioNet databases: the MIT-BIH Arrhythmia Dataset [73], [74], the MIT-BIH Normal Sinus Rhythm Dataset [73], and the BIDMC Congestive Heart Failure Dataset [73], [75]. Specifically, there were 96 recordings from persons with ARR, 30 recordings from persons with CHF, and 36 recordings from persons with NSR. The main objective was to develop a classifier that could accurately distinguish between the three categories: ARR, CHF, and NSR. Each raw ECG dataset had a signal length of 1 hour and was sampled at 128 Hz.

B. PROPOSED APPROACH

The main block diagram presented in Figure 1 illustrates the sequential flow of the EEG and ECG data, starting from signal acquisition through pre-processing, compressive sensing with OWHT, and finally, classification. Each step contributes to the overall analysis and understanding of the EEG and ECG signals, enabling efficient processing, feature extraction, and classification.

1) PRE-PROCESSING

The recorded EEG and ECG signals underwent several pre-processing steps to enhance their quality and remove unwanted artifacts. Firstly, a notch filter was applied to eliminate the 50-Hz frequency component caused by power supply interference. Subsequently, a first-order Butterworth filter was employed with a frequency range of 0.5 to 60 Hz to further refine the signals. To ensure consistency and improve detection efficiency across participants, feature normalization was performed on the extracted features from the signals. This normalization process involved scaling the feature values between 0 and 1 using min-max normalization. By adjusting the range of the features to a standardized scale, comparability and further analysis were facilitated. Finally, the pre-processed signals were segmented into non-overlapping segments of 1-second duration. This segmentation enabled the analysis of specific time intervals within the signals, aiding in the identification of patterns, events, or abnormalities. Through the combination of these pre-processing steps.

2) COMPRESSIVE SENSING PROPOSED ALGORITHM

Most traditional biomedical signal compressive sensing methods do not fully consider the presence of noise, particularly impulsive noise. While these methods often assume the presence of Gaussian noise, real-world compressed biomedical signals are frequently contaminated by impulsive noise. Impulsive noise can occur due to various factors such as missing data during measurement, transmission issues, buffer overflow, or faulty memory locations. When both Gaussian and impulsive noise affect the compressive sensing system at the sensor level, the resulting compressed biomedical signal becomes contaminated. To address this issue, it is necessary to include both Gaussian and impulsive noise in the signal measurement model. Mathematically, the measurement model can be represented as follows [76]:

$$Y = \phi X + G_n + IM_n \tag{1}$$

In the presence of both Gaussian noise (G_n) and impulsive noise (IM_n). The Frobenius norm of a matrix is commonly used to estimate Gaussian noise using maximum likelihood estimation. However, impulsive noise affects only a small percentage of the EEG signal but with a large error, and it exhibits a sparse property that can be characterized using the l_0 norm. To address these considerations, we can formulate the optimization model as follows:

$$\widehat{X} = \min_{X, G_n, IM_n} \|\Omega X\|_0 + \alpha \|G_n\|_F^2 + \beta \|IM_n\|_0 \tag{2}$$

In order to simplify the optimization problem, we can substitute the original l_0 norm with the l_1 norm, which is a convex relaxation of the l_0 norm. This substitution helps overcome the computational challenges associated with the non-convexity of the l_0 norm, which is typically NP-hard. The reformulated problem can be represented as follows:

$$\widehat{X} = \min_{X, G_n, IM_n} \|\Omega X\|_1 + \alpha \|G_n\|_F^2 + \beta \|IM_n\|_1 \tag{3}$$

In previous research conducted by Dauwels et al. [77] and Liu et al. [57], the effectiveness of employing low-rank approximation through matrix/tensor decomposition on EEG matrix/tensor for multichannel EEG compression was demonstrated. This approach utilized matrix/tensor decomposition techniques to exploit the underlying correlation among the multichannel EEG signals, revealing a latent low-rank property in the data. Building upon this observation, the reformulated equation 3 can be expressed as follows:

$$\widehat{X} = \min_{X, G_n, IM_n} \|\Omega X\|_1 + \lambda \, rank(X) + \alpha \|G_n\|_F^2 + \beta \|IM_n\|_1 \tag{4}$$

Here, $\mathbf{X}$ represents the low-rank approximation of the multichannel EEG matrix/tensor, while $\mathbf{Y}$ denotes the observed measurements. The term $|\mathbf{Y} - \Phi\mathbf{X}|F^2$ measures the fidelity between the observed measurements and the reconstructed low-rank approximation, aiming to minimize the discrepancy. The second term, $\alpha|\mathbf{X}|$, promotes low-rankness by encouraging a small nuclear norm ($|\mathbf{X}|$) of $\mathbf{X}$. The nuclear norm acts as a convex relaxation of the rank operator and effectively captures the low-rank structure present in the multichannel EEG data. Additionally, the third term, $\beta|\mathbf{X}|_1$, fosters sparsity by encouraging a small l_1 norm ($|\mathbf{X}|_1$) of $\mathbf{X}$, thereby capturing impulsive noise in the signals. By incorporating low-rank approximation through

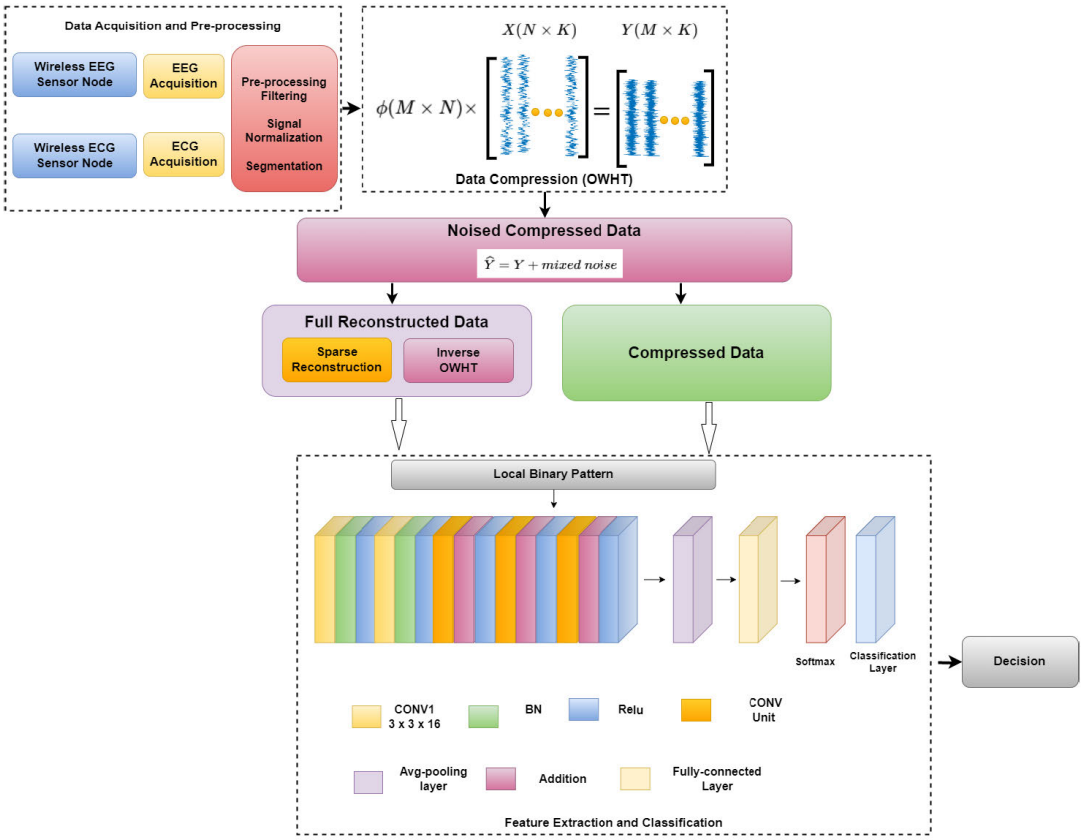

FIGURE 1. Block diagram corresponding to the proposed framework.

matrix/tensor decomposition and leveraging the nuclear norm and l_1 norm for regularization, this reformulated formulation facilitates accurate and efficient recovery of the multichannel EEG data. It effectively utilizes the latent low-rank property and captures the presence of impulsive noise, thereby enhancing the performance of multichannel EEG compression.

In this optimization model, the regularization parameter λ is used and the rank function about X is denoted as $rank(X)$. To substitute the rank function, the nuclear norm is adopted because it is widely used as a convex relaxation of the rank function [78]. Hence, the proposed optimization model based on sparse and low-rank representation can be formulated as follows:

$$\widehat{X} = \min_{X, G_n, IM_n} \|\Omega X\|_1 + \lambda \|X\|_* + \alpha \|G_n\|_F^2 + \beta \|IM_n\|_1 \tag{5}$$

The nuclear norm of a matrix X, denoted by $\|X\|_*$, is defined as the sum of its singular values. Due to the high correlation between nearby EEG channels, which is caused by both the shared sources of neural activities and the volume conduction effect, these signals exhibit similar patterns in the transform (sparsifying) domain. Specifically, high values in the transform domain occur in the same positions for these signals, resulting in a row-sparse matrix X. Therefore, taking advantage of these correlations in the reconstruction process can lead to high accuracy in the recovery procedure [79].

3) SELECTING THE MATRICES FOR SENSING AND SPARSIFICATION

To ensure accurate recovery in compressive sensing of biomedical signals, it is crucial to have a low mutual coherence value between the measurement matrix and sparsity matrix. Random matrices with independent identically distributed (i.i.d.) entries are well-known for their low coherence values when compared to deterministic matrices. Two popular random sensing matrices used in compressive sensing of biomedical signals are random Gaussian matrices and random binary matrices. Random Gaussian matrices have been widely employed in compressive sensing of EEG signals; however, they can be computationally expensive and not energy-efficient for use in WBAN systems. On the other hand, random binary sensing matrices offer computational efficiency and lead to small-size batteries for sensor nodes, making them suitable for WBAN systems. Previous studies have utilized random binary matrices as measurement matrices for compressive sensing of EEG signals. In terms of sparsity domains, original EEG signals are not sparse or compressible in the time domain. However, they can be

Algorithm 1 Biomedical Signal Compressed Sensing Using SPGL1 Algorithm and OWHT

Input: y - measured signal, Ω - measurement matrix, λ - sparsity penalty parameter, α - regularization parameter for the Frobenius norm term, β - regularization parameter for the image model term.

Output: $\hat{X}$ - reconstructed signal.

1: Initialize X_0 with random values
2: Set $k = 0$
3: Set $r_0 = y - \Omega X_0$
4: **while** $k \leq k_{max}$ and $|r_k| \geq \epsilon |y|$ **do**
5: Apply Optimized Walsh-Hadamard Transform (OWHT) to X_k to obtain G_k and IM_k
6: Solve the optimization problem:

$$\min_{X, G_k, IM_k} \quad |\Omega X| 1 + \lambda |X| * + \alpha |G_k|_F^2 + \beta |IM_k| 1$$
$$\text{subject to} \quad X = OWHT^{-1}(G_k, IM_k) \tag{6}$$

7: Set $Xk + 1 = X$
8: Set $r_{k+1} = y - \Omega X_{k+1}$
9: Set $k = k + 1$
10: **end while**
11: $\hat{X} = X_k$

sparsely represented in domains such as wavelet, Gabor, discrete cosine transform (DCT), and the Walsh-Hadamard Transform (WHT). In this study, the WHT domain is chosen as the sparsity domain for EEG signals due to its efficient capture of high-frequency content in the signal. EEG and ECG signals typically exhibit energy at high frequencies, and the WHT is effective in capturing this energy in a sparse representation. Furthermore, the WHT offers the advantage of a simple hardware implementation, making it well-suited for low-power embedded systems like WBAN sensors [80]. This characteristic makes the WHT a desirable choice for compressive sensing applications in resource-constrained environments.

4) RECOVERY ALGORITHM

Compressive sensing is a powerful technique for acquiring and reconstructing signals from a small number of linear measurements. In the biomedical field, this can be particularly useful for reducing acquisition time and improving patient comfort during imaging and monitoring procedures. One popular method for signal reconstruction in compressed sensing is based on solving a sparse optimization problem, where the signal is assumed to have a sparse representation in some basis or dictionary. In this context, Algorithm 1 presents the main steps for the SPGL1 algorithm. It provides a computationally efficient and flexible approach to solving sparse optimization problems, allowing for the incorporation of additional constraints or regularization terms. In this algorithm, a series of optimization problems are solved iteratively to reconstruct the signal from its compressed measurements, using a combination of sparsity-promoting penalties and image model regularization.

In biomedical signal processing, it is common for signals to be corrupted by noise, including Gaussian noise and impulsive noise. To address this issue, the SPGL1 algorithm can be combined with the OWHT to reconstruct the signal while simultaneously suppressing noise.

The algorithm begins by initializing X_0 with random values, and setting the iteration counter k to zero. The difference between the measured signal and the current estimate, $r_k = y - \Omega X_k$, is calculated. The algorithm then enters a loop, continuing until the maximum number of iterations k_{max} is reached or the residual error $|r_k|$ is below a specified tolerance ϵ. At each iteration, the OWHT is applied to X_k to obtain two transformed signals: the Gaussian noise signal G_k and the impulsive noise signal IM_k. These signals are used in the optimization problem, subject to the constraint that X can be recovered from G_k and IM_k using the inverse OWHT.

$$\min_{X, G_k, IM_k} \quad |\Omega X| 1 + \lambda |X| * + \alpha |G_k|_F^2 + \beta |IM_k|_1$$
$$\text{subject to } X = OWHT^{-1}(G_k, IM_k) \tag{7}$$

The optimization problem includes four terms: the ℓ_1-norm of the product of Ω and the signal X, which encourages sparsity in X; the nuclear norm of X, which promotes low-rank solutions; the Frobenius norm of G_k, which penalizes Gaussian noise; and the ℓ_1-norm of IM_k, which penalizes impulsive noise. The constraint ensures that the recovered signal X can be expressed as a linear combination of G_k and IM_k. After solving the optimization problem, the estimate of the signal is updated to $X_{k+1} = X$. The residual error r_{k+1} is calculated, and the iteration counter is incremented. The output of the algorithm is the reconstructed signal, $\hat{X}$, which is equal to X_k after the final iteration. By suppressing noise and promoting sparsity and low-rank solutions, the algorithm can provide an accurate reconstruction of the signal from noisy measurements.

5) EEG AND ECG CLASSIFICATION IN COMPRESSIVE SENSING-BASED WBAN SYSTEMS

The proposed algorithm aims to classify compressed EEG and ECG signals by utilizing a combination of LBP features and a 1-D CNN model. The algorithm takes as input a compressed signal with a total of N samples. It also requires the specification of LBP parameters, namely P (the number of neighboring points to consider) and R (the radius of the circular neighborhood). Additionally, the algorithm requires CNN hyperparameters to be defined. To train and validate the model, the algorithm takes the training data $\mathcal{D}$ and validation data $\mathcal{V}$ as inputs. The training data is used to train the CNN model, while the validation data is used to evaluate the model performance and fine-tune the hyperparameters. For each input window of size W samples, the algorithm generates a prediction $\hat{y}$ using the trained CNN model. The prediction represents the classification label assigned to the

input window based on the learned features and patterns extracted from the compressed signal. By combining the discriminative power of LBP features and the ability of CNNs to learn hierarchical representations, the algorithm aims to achieve accurate classification results for compressed EEG and ECG signals. The proposed approach for classification in compressed EEG and ECG signals combines LBP features and a 1-D CNN model. The input to the approach is a compressed signal with N samples, LBP parameters P and R, CNN hyperparameters, training data $\mathcal{D}$, and validation data $\mathcal{V}$. The output is the prediction $\hat{y}$ for each input window of size W samples. To extract features, LBP is applied to each input window, capturing the local texture patterns of the signal. The LBP features are then reshaped into a 3D tensor of shape $(N - W + 1, W, C)$, where C represents the number of channels. This reshaped tensor serves as the input to the CNN model. The CNN model is designed with layers including convolution, activation, pooling, dropout, fully connected (FC), and output layers. The hyperparameters such as the number of filters (K), filter size (F), pooling size (P), dropout rate (D), number of hidden units in the FC layer (H), epochs (E), and learning rate (α) are initialized. In the proposed architecture, the input layer accepts a $32 \times 32 \times 3$ image, followed by a 3×3 convolutional layer with 16 filters. Padding is used in the convolutional layer to maintain the original spatial dimensions. Batch normalization is applied to normalize the output, and the ReLU activation function is employed. The model incorporates residual blocks, each comprising two convolutional layers and an additional layer that adds the output of the second convolutional layer to the input. The number of filters in each convolutional layer is determined by the hyperparameter 'netWidth'. Batch normalization and ReLU activation are applied to the output of the second convolutional layer. Another 3×3 convolutional layer with the same number of filters is added, followed by another round of batch normalization, addition to the input, and ReLU activation. The output of the residual blocks undergoes global average pooling, which computes the average of each feature map over its entire spatial extent, resulting in a $1 \times 1 \times n$ tensor. An FC layer with two output units representing the classes in the dataset follows this, and a softmax activation layer provides a probability distribution over the classes. During training, the CNN model is trained on the training data $\mathcal{D}$ for a specified number of epochs using the Adam optimizer with a learning rate of α. The hyperparameters of the CNN model are tuned using the validation set $\mathcal{V}$ and grid search. Different combinations of hyperparameters are evaluated, and the best-performing set is selected based on performance metrics. For seizure prediction, the input EEG signal x is divided into overlapping windows of size W samples with a step size of S samples. LBP features are extracted for each window, and the trained CNN model is used to obtain a seizure prediction. The predictions from all windows are combined to generate the final seizure prediction $\hat{y}$ for the entire EEG signal x. The algorithmic variables used in the approach include $N = 10000$ (number of samples in the input EEG signal), $W = 256$ (window size), $S = 500$ (step size), $P = 8$ (number of sampling points in LBP), $R = 1$ (radius in LBP), $K = 32$ (number of filters in the convolution layer), $F = 10$

Algorithm 2 1-D CNN-Based Epileptic Seizure Detection With Compressed EEG and Local Binary Pattern (LBP) Features

1: **Input:** Compressed EEG signal x with N samples, LBP parameters P and R, CNN hyperparameters, training data $\mathcal{D}$, and validation data $\mathcal{V}$
2: **Output:** Seizure prediction $\hat{y}$ for each input window of size W samples
3: Extract LBP features for each input window of size W samples
4: Reshape the LBP features into a 3D tensor of shape $(N - W + 1, W, C)$
5: Define a 1-D CNN model with the following layers:
- Convolution layer with K filters of size F
- ReLU activation function: $f(x) = \max(0, x)$
- MaxPooling layer of size P
- Dropout layer with dropout rate D
- FC layer with H hidden units and ReLU activation function: $f(x) = \max(0, x)$
- FC output layer with a single output unit and sigmoid activation function: $f(x) = \frac{1}{1+e^{-x}}$

6: Initialize the CNN model hyperparameters
7: Train the CNN model on the training data $\mathcal{D}$ for E epochs using the Adam optimizer with learning rate α
8: Tune the hyperparameters of the CNN model using the validation set $\mathcal{V}$ and grid search:
9: Define a set of hyperparameters to search over, including K, F, P, D, H, E, and α
10: For each combination of hyperparameters, train the CNN model on $\mathcal{D}$ for E epochs and evaluate its performance on $\mathcal{V}$ using a suitable metric
11: Select the hyperparameters with the best performance on $\mathcal{V}$
12: Use the trained CNN model to classify EEG and ECG in the input signal x as follows:
13: Split the signal x into overlapping windows of size W samples with a step size of S samples
14: For each window, extract the LBP features and pass them through the trained CNN model to obtain prediction: $\hat{y}i = f\ (\text{CNN}\theta(x_i))$
15: Combine the predictions from all windows to obtain the final prediction $\hat{y}$ for the entire signal x: $\hat{y} = [\hat{y}_1, \hat{y}_2, \ldots, \hat{y}_M]$, where $M = \left\lfloor \frac{N-W}{S} \right\rfloor + 1$

where:

- x is a compressed EEG signal with N samples.
- W is the window size used for extracting LBP features and making predictions.
- S is the step size used for overlapping windows.

- P and R are parameters for the LBP algorithm, controlling the number of sampling points and the radius of the circle around each point.
- K is the number of filters used in the convolution layer of the CNN model.
- F is the size of each filter used in the convolution layer of the CNN model.
- P is the size of the max pooling layer of the CNN model.
- D is the dropout rate used in the dropout layer of the CNN model.

C. PERFORMANCE METRICES

In many studies of EEG compressed sensing, the Mean Squared Error (MSE) and the Maximum Correntropy Criterion (MCC) are often used to quantitatively evaluate the performance of compressive sensing recovery of multichannel EEG signals. The MSE measures the average squared difference between the estimated EEG signal $\hat{X}_l$ and the true EEG signal X_l in each segment. It can be formulated as:

$$MSE = \sum_{l=1}^{L} \frac{\left\| \hat{X}_l - X_l \right\|_F^2}{L \times N \times R} \tag{8}$$

where $X_l \in \mathbb{R}^{N \times R}$ represents the true EEG data with R channels and each channel has a length of N. The variable $\hat{X}_l$ denotes the estimated signal in the lth segment, and L is the total number of EEG segments. A lower MSE value indicates better performance, as it means the estimated signal is closer to the true signal on average.

On the other hand, the MCC is used to estimate the structural similarity between the estimated EEG signal and the true EEG signal. It is calculated by computing the inner product between the vectorized versions of the estimated and true EEG signals and normalizing it with the Frobenius norms of the signals. Mathematically, the MCC can be formulated as:

$$MCC = \sum_{l=1}^{L} \frac{\text{vec}(X_l)^T \text{vec}(\hat{X}_l)}{L \left\| X \right\|_F \left\| \hat{X}_l \right\|_F} \tag{9}$$

Here, vec() converts all columns in the matrix into a column vector. A higher MCC value indicates that the recovered EEG signal is more similar to the original signal. Both the MSE and MCC are commonly used metrics in biomedical signals compressed sensing studies to assess the quality of the recovery process. Researchers rely on these metrics to compare different algorithms, optimize parameters, and evaluate the effectiveness of compressive sensing techniques in the context of multichannel EEG signal recovery.

In addition, the subsampling ratio (SSR) is often used to measure the degree of compression and is defined as:

$$\text{SSR} = \frac{M}{N} \times 100 \tag{10}$$

where N and M denote the number of rows in the original signal X and compressed signal Y, respectively.

TABLE 1. Confusion matrix.

	Actually positive (1)	Actually negative (0)
Predicted positive	T_ps	F_ps
Predicted negative	F_ns	T_ns

QS represents the quality score of the estimated EEG signal compared to the true signal. It is calculated by normalizing the MSE with respect to the maximum possible value of the signal. A higher QS value indicates better quality, as it means the estimated signal has less error compared to the maximum possible value.

$$QS = 1 - \frac{MSE}{\text{MAX}^2} \tag{11}$$

The Peak Signal-to-Noise Ratio (PSNR) is a commonly used metric to measure the quality of the estimated EEG signal compared to the true signal. It represents the ratio of the maximum possible power of the signal to the power of the error.

$$PSNR = 10 \log_{10} \left(\frac{\text{MAX}^2}{MSE} \right) \tag{12}$$

where MAX denotes the maximum possible value of the EEG signal.

The Structural Similarity Index (SSIM) is a metric that assesses the structural similarity between the estimated EEG signal and the true signal.

$$SSIM = \frac{2\mu_{\hat{X}}\mu_X + C_1}{\mu_{\hat{X}}^2 + \mu_X^2 + C_1} \cdot \frac{2\sigma_{\hat{X}X} + C_2}{\sigma_{\hat{X}}^2 + \sigma_X^2 + C_2} \tag{13}$$

where $\mu_{\hat{X}}$ and μ_X represent the means of the estimated and true EEG signals, respectively. $\sigma_{\hat{X}}$ and σ_X represent the standard deviations of the estimated and true EEG signals, respectively. $\sigma_{\hat{X}X}$ represents the covariance between the estimated and true EEG signals. C_1 and C_2 are small constants added for numerical stability.

The performance of the deep learning classifier is evaluated using various metrics, including sensitivity (*Sen*), specificity (*Spec.*), accuracy (*Acc.*), precision (*Preci.*), and F_1 score [81], which are computed using a confusion matrix. Table 3 displays the anticipated quadrant outputs from the confusion matrix, with true positives (T_p) representing the number of correctly identified anomalous instances and true negatives (T_n) indicating the number of accurately classified normal instances. False positives (F_p) are normal instances that are incorrectly labeled as anomalies, while false negatives (F_n) are anomalies that are misclassified as normal.

Sensitivity is given by:

$$Sen. = \frac{T_p}{T_p + F_n} \times 100 \tag{14}$$

Specificity is given by:

$$Spec. = \frac{T_n}{T_n + F_p} \times 100 \tag{15}$$

TABLE 2. Comparison of compressive sensing recovery algorithms at different SSR using noise-free EEG signals.

SSR		0.1	0.2	0.3	0.4	0.5	0.6	0.7	0.8
MSE (10^{-3})	BSBL [6]	0.42	0.42	0.42	0.49	0.49	0.53	0.54	0.78
	KCS [58]	0.39	0.39	0.39	0.43	0.43	0.51	0.55	0.66
	RBCS [59]	0.30	0.31	0.32	0.34	0.35	0.36	0.42	0.68
	SCLR [57]	0.24	0.25	0.26	0.30	0.30	0.31	0.36	0.54
	SLRMN [60]	0.23	0.24	0.24	0.26	0.28	0.31	0.35	0.47
	Proposed OWHT	0.11	0.11	0.11	0.12	0.12	0.15	0.19	0.21
MCC	BSBL [6]	0.75	0,77	0.78	0.81	0.81	0.82	0.82	0.80
	KCS [58]	0.81	0.85	0.86	0.86	0.86	0.87	0.85	0.85
	RBCS [59]	0.70	0.71	0.71	0.72	0.72	0.72	0.72	0.71
	SCLR [57]	0.65	0.67	0.68	0.68	0.68	0.69	0.66	0.65
	SLRMN [60]	0.74	0.78	0.80	0.82	0.83	0.84	0.81	0.80
	Proposed OWHT	0.92	0.93	0.95	0.98	0.98	0.98	0.97	0.97

Accuracy is given by:

$$Acc. = \frac{T_p + T_n}{T_p + T_n + F_p + F_n} \times 100 \tag{16}$$

F_1 score is given by:

$$F_1\ score = \frac{T_p}{T_p + \frac{1}{2}(F_p + F_n)} \times 100 \tag{17}$$

The F_1 score, also called the F-measure, is a useful metric for evaluating the accuracy of a test. To compute the F_1 score, one divides the number of true positive results by the total number of positive results, which includes both true and false positives. Meanwhile, the recall assesses the number of correctly identified positive results in relation to the total number of positive samples. The F_1 score is obtained by taking the harmonic mean of precision and recall, as detailed in [82].

IV. RESULTS AND DISCUSSION

The presented framework for detecting EEG and ECG signals in the compressed sensing domain is evaluated in two scenarios: compression and classification. We begin by assessing the performance of the proposed compression algorithm on EEG and ECG signals.

A. RESULTS FOR EEG COMPRESSION IN THE ABSENCE OF NOISE

Table 2 provides a comprehensive comparison of six different algorithms used for compressive sensing recovery, namely BSBL, KCS, RBCS, SCLR, SLRMN, and the proposed OWHT algorithm. The table showcases the performance of each algorithm based on two key metrics, namely MSE and MCC. MSE values are expressed in units of 10^{-3}, where smaller values indicate better performance in approximating the original signal. On the other hand, MCC values range from 0 to 1, where 1 signifies a perfect correlation between the predicted and actual values. Upon analyzing the results in the table, it becomes evident that the proposed OWHT algorithm surpasses all other algorithms in terms of both

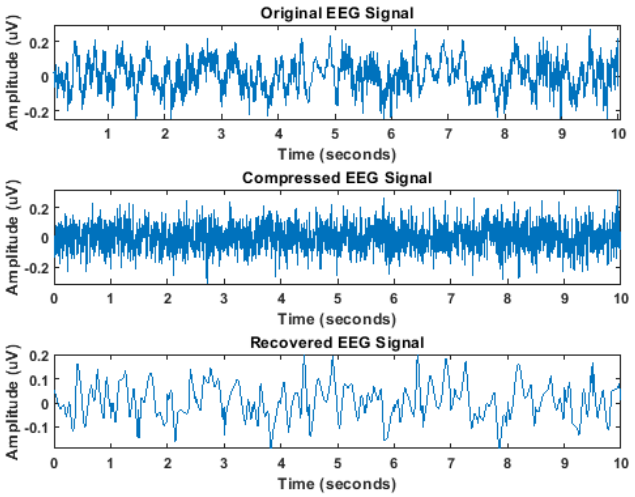

FIGURE 2. Comparison of original EEG signal, compressed EEG, and recovered EEG in the absence of noise.

MSE and MCC metrics. At various levels of SSR, ranging from 0.1 to 0.8 with increments of 0.1, the OWHT algorithm consistently demonstrates the lowest MSE values and the highest MCC values. This consistent performance across different SSR levels highlights the efficacy of the proposed algorithm in accurately reconstructing signals from compressed measurements. Additionally, the SLRMN algorithm also exhibits competitive performance, particularly at higher SSR levels, where it achieves commendable MCC values. However, the BSBL algorithm lags behind the others, yielding higher MSE values and lower MCC values across all SSR levels, suggesting relatively inferior reconstruction performance. Figure 2 showcases a visual representation of the key stages in the compressive sensing-based EEG signal processing. It includes the original EEG signal, the compressed EEG signal, and the recovered EEG signal. The original EEG signal represents the raw electrical activity recorded from the brain, free from any added noise or distortion. As the ground truth reference, it provides insight into the true underlying brain activity. The compressed EEG signal is obtained by employing compressive sensing techniques, enabling efficient data acquisition and storage through the exploitation of signal sparsity or compressibility. This compressed version of the EEG signal contains a reduced amount of data compared to the original signal, resulting in more efficient signal transmission and storage. The recovered EEG signal is the outcome of applying a novel compressive sensing recovery algorithm to the compressed EEG signal. This algorithm is designed to reconstruct the original EEG signal from the compressed measurements, aiming to capture and restore essential features and information present in the signal. By visually examining Figure 2, one can assess the performance of the compressive sensing recovery algorithm by comparing the recovered signal with the original EEG signal. A high degree of similarity between the recovered and original signals indicates a successful recovery, affirming

TABLE 3. Performance comparison of compressive sensing algorithms on EEG signals corrupted with 30 dB White Gaussian Noise.

SSR		0.1	0.2	0.3	0.4	0.5	0.6	0.7	0.8
MSE (10^{-3})	BSBL [6]	0.44	0.46	0.46	0.49	0.50	0.54	0.62	0.73
	KCS [58]	0.42	0.43	0.44	0.47	0.48	0.53	0.62	0.66
	RBCS [59]	0.33	0.35	0.40	0.40	0.40	0.40	0.54	0.73
	SCLR [57]	0.25	0.25	0.27	0.28	0.31	0.37	0.48	0.54
	SLRMN [60]	0.27	0.28	0.31	0.33	0.36	0.38	0.45	0.53
	Proposed OWHT	0.17	0.17	0.18	0.18	0.19	0.19	0.23	0.27
MCC	BSBL [6]	0.73	0.75	0.76	0.79	0.79	0.80	0.80	0.81
	KCS [58]	0.78	0.82	0.83	0.85	0.85	0.86	0.86	0.86
	RBCS [59]	0.68	0.68	0.68	0.70	0.70	0.70	0.71	0.72
	SCLR [57]	0.63	0.64	0.65	0.65	0.65	0.65	0.69	0.70
	SLRMN [60]	0.72	0.75	0.78	0.79	0.80	0.81	0.85	0.88
	Proposed OWHT	0.90	0.91	0.94	0.96	0.97	0.97	0.98	0.98

the algorithm's accuracy and effectiveness. Conversely, significant discrepancies may suggest potential limitations or inaccuracies in the recovery process.

B. RESULTS FOR EEG COMPRESSION IN PRESENCE OF GAUSSIAN NOISE

In this section, we present the results of the proposed compressive sensing algorithm for EEG signal denoising in the presence of Gaussian noise at a 30 dB level. Table 3 summarizes the performance evaluation using two essential metrics, MSE and MCC. The table is divided into two sections: the upper section presents the MSE values, while the lower section displays the MCC values. Each column corresponds to a specific SSR level, ranging from 0.1 to 0.8, and each row corresponds to a different denoising algorithm, including BSBL, KCS, RBCS, SCLR, SLRMN, and the proposed OWHT algorithm. Analyzing the MSE values, it is evident that the proposed OWHT algorithm consistently outperforms the other methods across all noise levels. This noteworthy performance indicates the effectiveness of the OWHT algorithm in denoising EEG signals and preserving their quality, even when exposed to significant noise levels. Moving on to the MCC values, the proposed OWHT algorithm again exhibits superior performance compared to the other methods. This finding implies that the OWHT algorithm not only effectively removes noise but also enhances the accuracy of EEG signal analysis and interpretation. The high MCC values suggest that the OWHT algorithm provides reliable results in capturing relevant features and patterns in the EEG data, even amidst the presence of noise.

Figure 3 provides valuable insights into the performance of the compression and recovery process for the EEG signal in the presence of 30 dB WGN. The original EEG signal serves as the baseline, representing the true underlying brain activity. Introducing 30 dB WGN to the original signal simulates real-world scenarios where EEG signals are often subject to various sources of interference or noise. The compressed EEG signal is the outcome of applying the compression algorithm to the original noisy signal. This subplot showcases

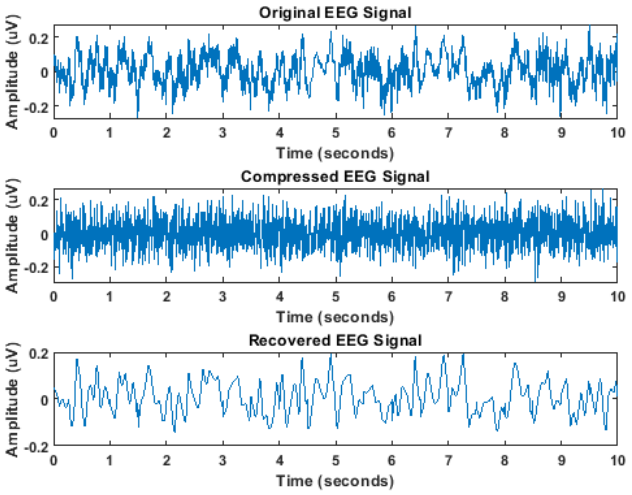

FIGURE 3. Comparison of original EEG signal with 30 dB WGN, compressed EEG, and recovered EEG.

the reduction in data size achieved through compression, which is crucial for efficient storage and transmission of EEG signals. However, it is essential to note that the compression process may lead to the loss of some fine-grained details present in the original signal due to data reduction. The recovered EEG signal is obtained by reconstructing the compressed signal using the recovery algorithm. This subplot demonstrates the effectiveness of the recovery algorithm in restoring the original EEG signal, despite the presence of noise and the loss incurred during compression. The accuracy and similarity between the recovered signal and the original signal indicate the algorithm's ability to successfully capture and reconstruct the essential features of the EEG signal. By comparing the original EEG signal, the compressed EEG signal, and the recovered EEG signal, one can thoroughly assess the fidelity of the recovery process. If the recovered signal closely resembles the original signal, it indicates a successful recovery, and the compression algorithm has effectively preserved the crucial information required for subsequent analysis or interpretation.

C. RESULTS FOR EEG COMPRESSION IN PRESENCE OF IMPULSIVE NOISE

Table 4 presents a comprehensive performance evaluation of various algorithms based on two essential evaluation metrics. The comparison is conducted under different levels of compression ratios, ranging from 0.1 to 0.8, for EEG signal data. For the SSR metric, it is evident that most of the algorithms exhibit an increasing trend in MSE values as the compression ratio rises. However, the proposed OWHT algorithm stands out by consistently outperforming the other algorithms. Across all compression ratios, the OWHT algorithm showcases significantly lower MSE values. This noteworthy result indicates that the proposed OWHT algorithm excels in preserving the quality of the EEG signal, even at higher compression ratios, compared to competing

TABLE 4. Performance comparison of compressive sensing algorithms on EEG signals corrupted with 0.05 impulsive Noise.

SSR		0.1	0.2	0.3	0.4	0.5	0.6	0.7	0.8
MSE (10^{-3})	BSBL [6]	0.61	0.62	0.63	0.63	0.64	0.66	0.68	0.72
	KCS [58]	0.60	0.60	0.60	0.64	0.67	0.68	0.68	0.74
	RBCS [59]	0.63	0.65	0.70	0.70	0.70	070	0.74	0.83
	SCLR [57]	0.55	0.55	0.57	0.58	0.61	0.67	0.68	0.74
	SLRMN [60]	0.47	0.48	0.51	0.53	0.56	0.58	0.65	0.73
	Proposed OWHT	0.19	0.19	0.19	0.19	0.20	0.20	0.25	0.29
MCC	BSBL [6]	0.71	0.73	0.73	0.75	0.76	0.78	0.78	0.80
	KCS [58]	0.76	0.77	0.77	0.77	0.78	0.80	0.84	0.84
	RBCS [59]	0.65	0.65	0.65	0.68	0.68	0.68	0.68	0.68
	SCLR [57]	0.60	0.60	0.60	0.60	0.60	0.60	0.65	0.68
	SLRMN [60]	0.70	0.70	0.75	0.75	0.75	0.78	0.78	0.80
	Proposed OWHT	0.89	0.90	0.93	0.96	0.97	0.97	0.97	0.97

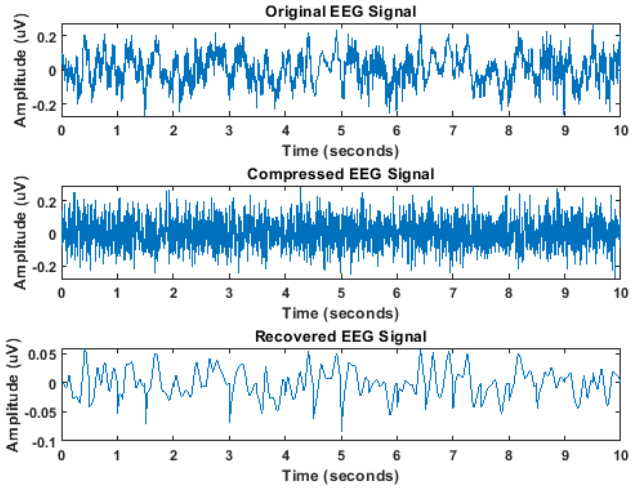

FIGURE 4. Comparison of original EEG signal with 0.05 impulsive noise, compressed EEG, and recovered EEG.

methods like BSBL, KCS, RBCS, SCLR, and SLRMN. Likewise, for the MCC metric, the proposed OWHT algorithm demonstrates remarkable performance. It consistently achieves higher MCC values than the other algorithms, indicating its superior accuracy in recovering the original EEG signal during the compression and reconstruction process. The consistently high MCC values for the OWHT algorithm further emphasize its efficacy in retaining the critical features of the EEG signal throughout the compression and recovery stages. These comprehensive results collectively suggest that the proposed OWHT algorithm exhibits robustness and accuracy in compressing and recovering EEG signals. It outperforms the other algorithms considered in terms of both MSE and MCC metrics, underscoring its potential as an efficient and effective solution for EEG signal compression and subsequent analysis. Figure 4 provides valuable insights into the impact of impulsive noise on the original EEG signal and the performance of the compression and recovery process. In this analysis, the original EEG signal is corrupted with 0.05 impulsive noise, and the subsequent steps involve applying a compression algorithm to obtain the compressed EEG signal, followed by reconstructing the signal to obtain the recovered EEG signal. Upon observation, it becomes apparent that the impulsive noise introduces irregular and abrupt spikes in the original EEG signal. These spikes disrupt the underlying patterns and pose challenges in accurately interpreting the signal. However, despite the presence of impulsive noise, the compression algorithm effectively reduces the size of the signal while preserving essential information. The compressed EEG signal showcases a reduced amplitude and a smoother profile compared to the original signal. Although some fine-grained details may be lost during the compression process, the overall shape and structure of the signal are well-maintained, resulting in a reasonable representation of the original EEG. Notably, the recovered EEG signal, obtained through the reconstruction process, exhibits a remarkable similarity to the original signal, even in the presence of impulsive noise. While some noise artifacts may persist, the key features and underlying patterns of the original EEG signal are successfully recovered.

TABLE 5. Performance comparison of compressive sensing algorithms on EEG signals corrupted with Mixed Noise.

SSR		0.1	0.2	0.3	0.4	0.5	0.6	0.7	0.8
MSE (10^{-3})	BSBL [6]	0.65	0.65	0.65	0.66	0.66	0.67	0.67	0.74
	KCS [58]	0.62	0.62	0.62	0.63	0.64	0.68	0.70	0.76
	RBCS [59]	0.65	0.65	0.67	0.72	0.73	073	0.77	0.85
	SCLR [57]	0.57	0.55	0.57	0.58	0.61	0.67	0.68	0.74
	SLRMN [60]	0.47	0.48	0.51	0.53	0.56	0.58	0.65	0.73
	Proposed OWHT	0.19	0.19	0.20	0.20	0.22	0.22	0.27	0.32
MCC	BSBL [6]	0.70	0.70	0.70	0.73	0.73	0.75	0.77	0.78
	KCS [58]	0.73	0.73	0.74	0.74	0.76	0.76	0.77	0.80
	RBCS [59]	0.62	0.62	0.63	0.63	0.65	0.65	0.67	0.67
	SCLR [57]	0.56	0.56	0.56	0.56	0.58	0.58	0.59	0.62
	SLRMN [60]	0.67	0.67	0.68	0.69	0.69	0.73	0.77	0.79
	Proposed OWHT	0.89	0.90	0.93	0.96	0.97	0.97	0.97	0.97

D. RESULTS FOR EEG COMPRESSION IN PRESENCE OF MIXED NOISE

Table 5 demonstrates that the OWHT algorithm consistently outperforms other compression algorithms in handling mixed noise in EEG signals. It achieves lower mean MSE values, indicating effective noise reduction and preservation of the original signal. Moreover, OWHT obtains higher MCC values, showcasing better classification performance and preservation of essential signal features. On the other hand, the other compression algorithms exhibit higher MSE values and lower MCC values across various compression ratios. These results validate the efficacy of the OWHT algorithm in enhancing the quality of compressed EEG signals corrupted with mixed noise, making it a promising approach for EEG signal compression.

Figure 5 depicts the impact of mixed noise (30 dB WGN and 0.05 impulsive noise) on the original EEG signal, along

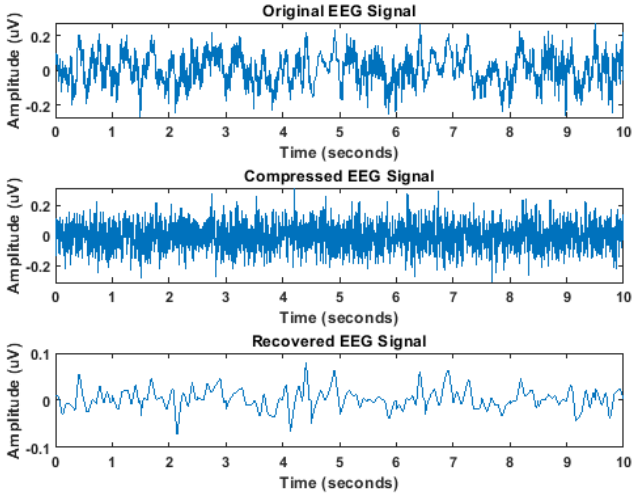

FIGURE 5. Comparison of original EEG signal with mixed noise, compressed EEG, and recovered EEG.

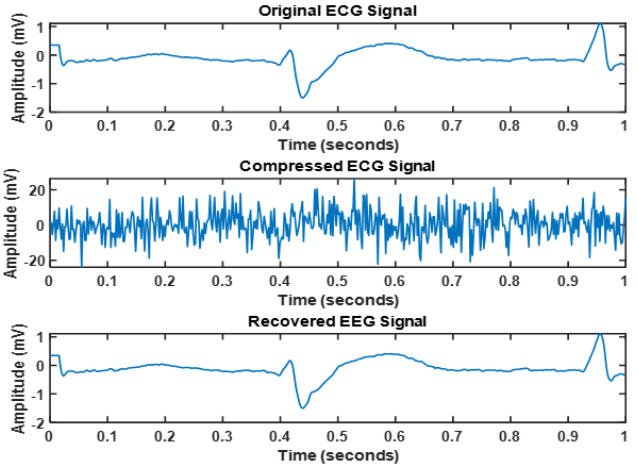

FIGURE 6. Comparison of original noise-free ECG signal, compressed ECG, and recovered ECG in the absence of noise.

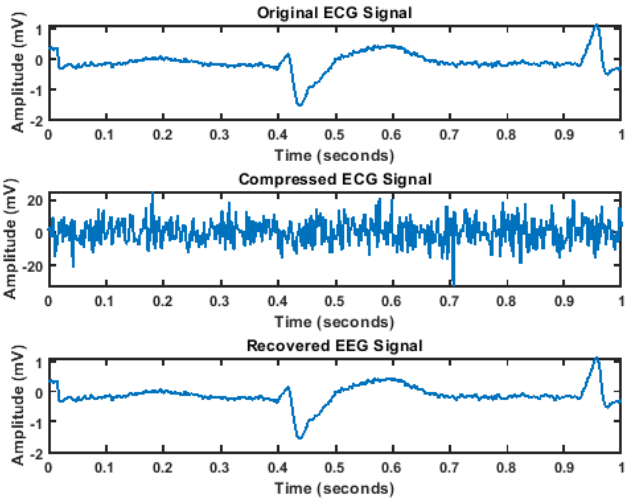

FIGURE 7. Comparison of original ECG signal, compressed ECG, and recovered ECG with added power line noise.

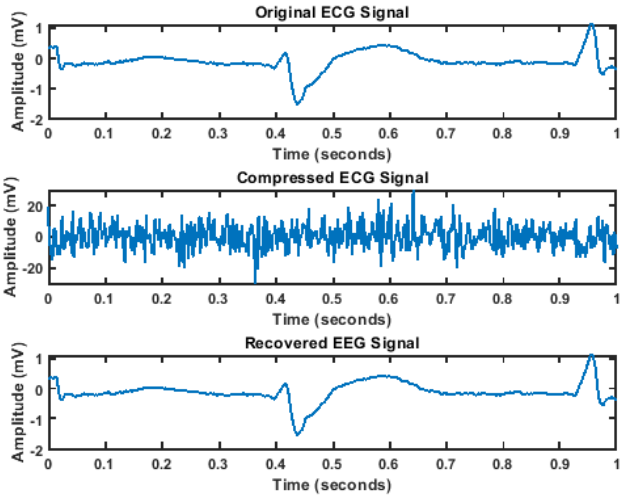

FIGURE 8. Comparison of original ECG signal, compressed ECG, and recovered ECG with added muscle artifact noise.

with the compression and recovery process. Despite the noise, the compression algorithm effectively reduces the signal size while preserving vital information. The recovered EEG signal shows a reasonable approximation of the original, enabling further analysis and interpretation.

Table 6 presents the performance evaluation of compressed EEG signals using various quality metrics. Results demonstrate the influence of SSR on compression efficiency, affecting metrics such as MSE, MCC, and qs. PSNR and SSIM values exhibit variations based on noise conditions and SSR values.

E. RESULTS FOR ECG COMPRESSION IN THE ABSENCE OF NOISE

In ECG compressive sensing, noise presents a critical challenge that can compromise the reconstruction quality and accuracy of compressed signals. Notably, muscle artifacts and power line interference are prominent noise sources. To address this, advanced signal processing techniques and noise reduction methods are incorporated during the reconstruction process. These measures effectively mitigate the impact of muscle artifacts and power line interference, leading to improved accuracy and fidelity in the reconstructed ECG signals. To simulate this noise, a sinusoidal waveform is added to the ECG signal at the corresponding frequency.

Figure 6 presents the comparison between the noise-free original ECG signal, its corresponding compressed version, and the reconstructed ECG signal. The figure highlights the fidelity and accuracy of the compressive sensing reconstruction process. The compressed ECG effectively retains crucial features of the original signal, while the reconstructed ECG closely resembles the noise-free version, indicating successful recovery of cardiac information. In Figure 7, we evaluate the impact of power line noise on the original ECG signal, compressed ECG, and the reconstructed ECG signal. The figure demonstrates the effectiveness of the

TABLE 6. Numerical evaluation results for different quality metrics of compressed EEG signals under noise-free and mixed noise conditions, with varying SSR values.

SSR	Noise free						Mixed noise					
	MSE (10^{-3})	MCC	T (sec)	qs	PSNR	SSIM	MSE (10^{-3})	MCC	T (sec)	qs	PSNR	SSIM
0.1	0.11	0.92	1.49	0.95	25.84	0.97	0.19	0.89	1.87	0.93	23.44	0.96
0.2	0.11	0.93	1.47	0.95	25.84	0.95	0.19	0.90	1.85	0.93	23.44	0.96
0.3	0.11	0.95	0.934	0.96	25.84	0.95	0.20	0.93	1.76	0.94	23.16	0.95
0.4	0.12	0.98	0.92	0.97	25.57	0.93	0.20	0.96	1.34	0.94	23.16	0.95
0.5	0.12	0.98	0.92	0.97	25.57	0.91	0.22	0.97	1.33	0.95	22.58	0.94
0.6	0.15	0.98	0.833	0.98	24.49	0.90	0.22	0.97	1.31	0.95	22.58	0.90
0.7	0.19	0.97	0.76	0.98	23.40	0.90	0.27	0.97	1.30	0.96	21.00	0.89
0.8	0.21	0.97	0.63	0.98	22.88	0.89	0.32	0.97	1.29	0.96	20.05	0.88

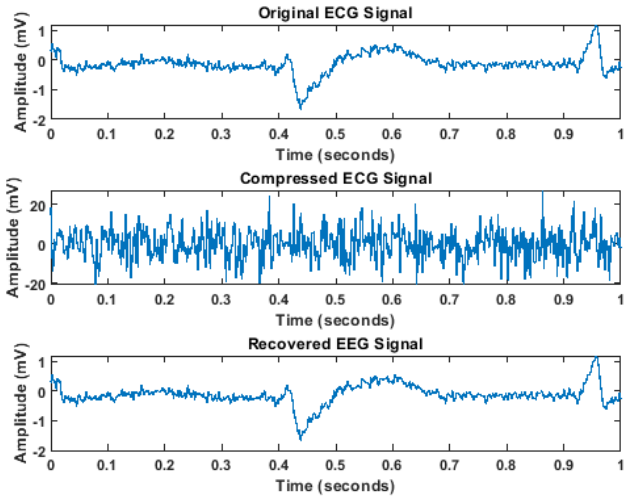

FIGURE 9. Comparison of original ECG signal, compressed ECG, and recovered ECG with added mixed noise.

TABLE 7. Performance evaluation of the proposed framework for compressive sensing algorithm on ECG signals corrupted with different types of noise.

SSR		0.1	0.2	0.3	0.4	0.5	0.6	0.7	0.8
MSE (10^{-3})	ECG noise free	0.11	0.11	0.12	0.12	0.13	0.14	0.17	0.22
	ECG+ power line noise	0.13	0.13	0.13	0.14	0.15	0.17	0.19	0.23
	ECG+ muscle artifact noise	0.14	0.14	0.15	0.15	0.15	0.18	0.18	0.25
	ECG+mixed noise	0.17	0.17	0.17	0.16	0.16	0.17	0.19	0.26
MCC	ECG noise free	0.95	0.95	0.96	0.97	0.99	0.99	0.99	0.99
	ECG+ power line noise	0.94	0.94	0.95	0.97	0.98	0.98	0.98	0.98
	ECG+ muscle artifact noise	0.93	0.93	0.94	0.95	0.96	0.97	0.97	0.97
	ECG+mixed noise	0.91	0.91	0.93	0.95	0.95	0.96	0.96	0.96

compressive sensing algorithm in mitigating power line interference. Despite the presence of noise, the compressed ECG accurately captures the underlying cardiac activity, and the reconstructed ECG exhibits a high level of similarity to the original signal, indicating successful noise removal. Figure 8 showcases the performance of the compressive sensing technique in handling muscle artifact noise. It compares the original ECG signal, compressed ECG, and reconstructed ECG in the presence of muscle artifacts. Despite the noise, the compressed ECG retains important cardiac features, and the reconstructed ECG successfully eliminates the artifacts, closely resembling the original ECG signal. Lastly, in Figure 9, we examine the capability of compressive sensing in handling mixed noise, including power line interference and muscle artifacts. Despite the challenging noise conditions, the compressed ECG preserves essential cardiac information, and the reconstructed ECG effectively removes the mixed noise, accurately capturing the underlying ECG waveform.

Table 7 provides a comprehensive comparison of performance metrics for different ECG signal scenarios, focusing on MSE and MCC evaluations. In the ECG noise-free scenario, MSE values range from 0.11 to 0.22 (10^{-3} units), with the lowest at an SSR of 0.1. This indicates accurate reconstruction of the noise-free ECG signal. The MCC values ranging from 0.95 to 0.99 further confirm successful ECG feature classification. In the presence of power line noise, the MSE values range from 0.13 to 0.23 (10^{-3} units). Despite the noise, the compressed ECG signals are accurately reconstructed, with MCC values ranging from 0.94 to 0.98, reflecting robust classification performance, slightly lower than the noise-free case. Considering muscle artifact noise, MSE values range from 0.14 to 0.25 (10^{-3} units). The compressive sensing algorithm effectively mitigates muscle artifacts, achieving accurate reconstruction with MCC values ranging from 0.93 to 0.97, indicating reliable classification performance. In the case of mixed noise (power line interference and muscle artifacts), MSE values range from 0.16 to 0.26 (10^{-3} units). The compressive sensing technique successfully reconstructs ECG signals, removing mixed noise, with MCC values ranging from 0.91 to 0.96, indicating robust classification performance in the presence of multiple noise sources. These results highlight the effectiveness of compressive sensing in accurately reconstructing ECG signals and maintaining reliable classification performance under challenging noise conditions. Low MSE values demonstrate preserved cardiac information, while high MCC values reflect accurate ECG feature detection. These findings support the suitability of compressive sensing for noise reduction and signal recovery in ECG analysis.

TABLE 8. Evaluation results for different quality metrics of compressed ECG signals under noise-free and mixed noise conditions, with varying SSR values.

SSR	Noise free						Mixed noise					
	MSE (10^-3)	MCC	T (sec)	qs	PSNR	SSIM	MSE (10^-3)	MCC	T (sec)	qs	PSNR	SSIM
0.1	0.11	0.95	1.45	0.96	26.84	0.98	0.17	0.91	1.77	0.94	24.44	0.965
0.2	0.11	0.95	1.44	0.96	26.84	0.98	0.17	0.91	1.75	0.94	24.44	0.963
0.3	0.12	0.96	0.834	0.97	26.84	0.97	0.17	0.93	1.54	0.94	23.46	0.958
0.4	0.12	0.97	0.82	0.97	26.57	0.97	0.16	0.95	1.44	0.95	23.46	0.956
0.5	0.13	0.99	0.82	0.97	26.57	0.95	0.16	0.96	1.43	0.95	22.58	0.944
0.6	0.14	0.99	0.811	0.98	23.49	0.93	0.17	0.97	1.35	0.95	22.58	0.92
0.7	0.17	0.99	0.74	0.98	23.40	0.92	0.19	0.97	1.33	0.96	22.00	0.90
0.8	0.22	0.99	0.65	0.98	21.88	0.92	0.26	0.97	1.31	0.96	21.05	0.90

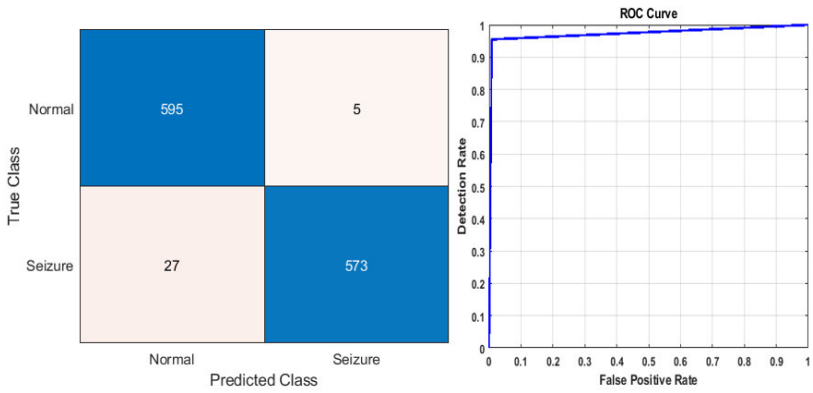

FIGURE 10. Confusion matrix and ROC curve for original EEG signal classification.

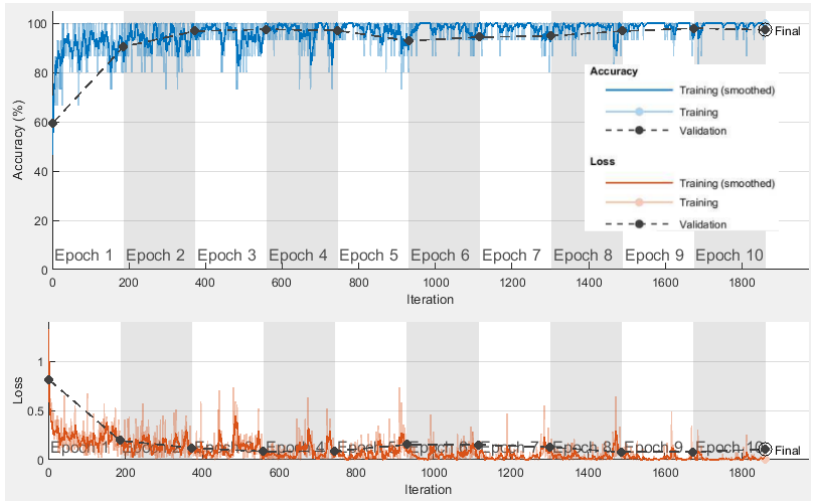

FIGURE 11. Training progress curve for the proposed CNN residual learning-based model with original EEG signal.

Table 8 further presents the performance evaluation of compressed ECG signals using various quality metrics. The consideration of noise-free and mixed noise scenarios, with varying SSR values, offers insights into compression efficiency. Higher SSR values generally lead to improved performance, evidenced by lower MSE, higher MCC, and higher qs. Additionally, PSNR and SSIM values provide valuable information about visual quality and similarity of compressed ECG signals.

F. RESULTS FOR EEG SEIZURE CLASSIFICATION USING THE PROPOSED CNN MODEL

In this section, we assess the efficacy of our proposed CNN-based approach for EEG classification across three distinct scenarios, highlighting the advantages of compressive sensing. Our model utilizes residual learning to classify the original EEG signals, the compressed EEG signals, and the fully reconstructed EEG signals.

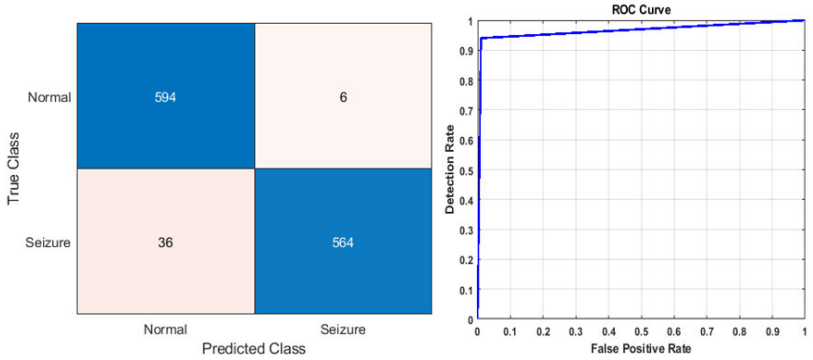

FIGURE 12. Confusion matrix and ROC curve for compressed EEG signal classification.

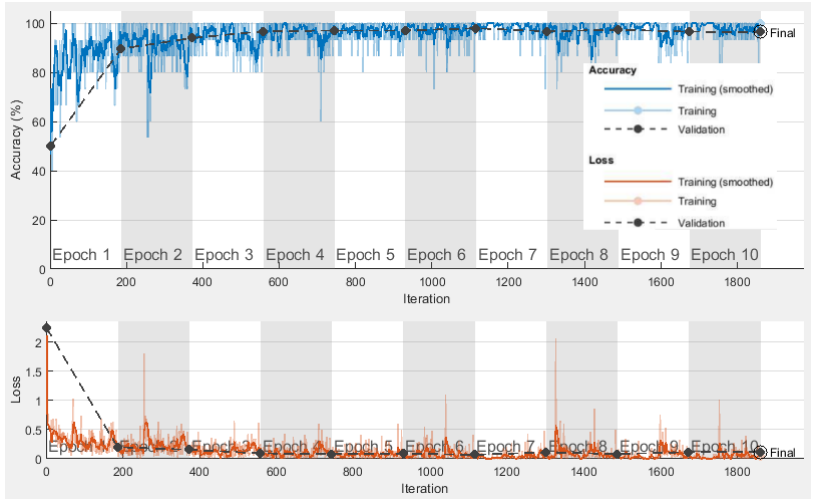

FIGURE 13. Training progress curve for the proposed CNN residual learning-based model with compressed EEG signal.

Figure 10 illustrates the confusion matrix and ROC curve for the classification of original EEG signals. The confusion matrix indicates that, out of 600 samples, the CNN model made 595 T_p predictions and 573 T_n predictions, demonstrating successful identification of positive and negative classes in most cases. The low numbers of $F_p = 5$ and $F_n = 27$ highlight the CNN model robustness in minimizing misclassifications. The ROC curve visually depicts the sensitivity-specificity trade-off. The curve's steep ascent from the origin and subsequent upward trend indicate that our CNN model achieved a high true positive rate while maintaining a low false positive rate. This confirms the model's excellent discriminatory power, enabling accurate differentiation between different classes of EEG signals. Furthermore, Figure 11 presents the training progress curve of the CNN model. By monitoring the loss function and accuracy metrics during training, we can observe the model's evolving performance. The curve's steady decrease in the loss function and simultaneous increase in accuracy signify the effective learning of underlying patterns and features in the original EEG signals, leading to improved classification performance. Note that for our experiments, we split the dataset into 80% for training and validation, and 20% for testing, to ensure reliable evaluations of the CNN model's performance.

The evaluation of the proposed CNN model on the classification of compressed EEG signals is presented in Figures 12 and 13. The confusion matrix shows that out of 600 samples, the model achieved 594 T_p predictions and 564 T_n predictions. However, there were also 6 F_p and 36 F_n, indicating some misclassifications. Analyzing the ROC curve provides insights into the model's ability to distinguish between different classes of compressed EEG signals. The curve indicates a reasonable discriminatory power, but there is potential for further improvement to optimize the trade-off between the true positive rate and false positive rate. The training progress curve illustrates the CNN model's learning process when trained on compressed EEG signals. Monitoring the loss function and accuracy metrics during training reveals the model's convergence and performance. A steady decrease in the loss function and corresponding increase in accuracy indicate effective learning

TABLE 9. Results for the proposed CNN model using EEG signals.

Model	Evaluation metrics (%)					
	Acc	Sen	Spec	Preci	F1score	Fpr
CNN+ original EEG	97.33	99.17	95.50	95.66	97.38	0.0450
CNN+compressed EEG	96.50	99.00	94.00	94.29	96.59	0.0600
CNN+fully reconstructed EEG	96.83	95.33	98.33	98.28	96.79	0.0167

TABLE 10. Results for the proposed CNN model using ECG signals.

Model	Evaluation metrics (%)					
	Acc	Sen	Spec	Preci	F1score	Fpr
CNN+ original ECG	95.78	95.78	97.89	96.00	95.81	0.0211
CNN+compressed ECG	92.89	92.89	96.44	93.78	92.99	0.0356
CNN+fully reconstructed ECG	94.89	94.89	97.44	95.03	94.91	0.0256

of relevant features from the compressed EEG signals. However, fluctuations or plateaus in the curves suggest the need for further adjustments or fine-tuning to enhance model performance.

The evaluation of the proposed CNN model for the classification of fully reconstructed EEG signals yields promising results, highlighting its strengths and advantages. Figure 14 presents the confusion matrix and ROC curve, providing valuable insights into the model's performance. The confusion matrix shows that the model achieved a high number of T_p and T_n predictions, indicating its ability to correctly classify instances. The ROC curve visually represents the trade-off between sensitivity and 1 - specificity. The curve steep ascent from the origin and subsequent upward trend indicate that the proposed CNN model achieved a high true positive rate while maintaining a low false positive rate. This suggests the model's excellent discriminatory power and its accurate differentiation between different classes of EEG signals. Additionally, Figure 15, which illustrates the training progress curve of the CNN model when trained on fully reconstructed EEG signals, provides further insights into the learning process. The consistent decrease in the loss function and the simultaneous increase in accuracy during training demonstrate the model's effective learning of relevant features from the fully reconstructed EEG signals. This indicates the model's capability to capture the important patterns and characteristics necessary for accurate classification.

Table 9 presents a comprehensive overview of the evaluation metrics for three scenarios used in EEG signal classification. For the CNN+ original EEG scenario, the model achieves an impressive accuracy of 97.33%, indicating accurate classification. The model also demonstrates excellent sensitivity 99.17%, specificity 95.50%, precision 95.66%, and F1 score 97.38%. The low false positive rate at 0.0450 highlights minimal misclassifications. The CNN+compressed EEG scenario achieves a slightly lower accuracy of 96.50% compared to the original EEG model. However, it maintains high sensitivity 99.00% and specificity 94.00%. The precision and F1 score are also high at 94.29% and 96.59%, respectively. The F_{pr} increases slightly to 0.0600, indicating a slightly higher misclassification rate compared to the original EEG model. The CNN+fully reconstructed EEG scenario achieves an accuracy of 96.83%, similar to other models. It demonstrates a sensitivity of 95.33% and an impressive specificity of 98.33%. The precision and F1 score are both high at 98.28% and 96.79%, respectively. The F_{pr} is remarkably low at 0.0167, indicating significantly reduced misclassifications compared to other models. Overall, the proposed CNN model showcases advantages in classifying fully reconstructed EEG signals, with high T_p and T_n rates, as demonstrated by the ROC curve. The model's learning process, depicted in the training progress curve, supports its ability to capture meaningful features. Despite a relatively small improvement of approximately 0.34% in accuracy for fully reconstructed EEG signals compared to compressed EEG signals, the added complexity and computational burden may not be justified. Hence, the CNN+compressed EEG model remains a more practical choice.

G. RESULTS FOR ECG CLASSIFICATION USING THE PROPOSED CNN MODEL

This study investigates the impact of compression on ECG classification performance through three scenarios: original ECG signals, compressed ECG signals, and fully reconstructed ECG signals. The original ECG signals serve as a baseline, representing uncompressed and unaltered data. In the compressed ECG scenario, signals undergo transformation using OWHT and subsequent compression to reduce data size. In the fully reconstructed ECG scenario, compressed signals are recovered using the SPGL1 algorithm and OWHT to reconstruct the original ECG signals. Figures 16 and 17 present the confusion matrix, ROC curve, and training progress curve for the CNN model using original ECG signals. Figures 18 and 19 present the same evaluation metrics for the CNN model using compressed ECG signals. Figures 20 and 21 present the evaluation metrics for the CNN model using fully reconstructed ECG signals.

Table 10 presents a comprehensive comparison of ECG classification scenarios, along with their evaluation metrics, providing valuable insights into the models' performance. In the CNN + original ECG scenario, the model achieves an accuracy of 95.78%, displaying precise ECG signal classification. Sensitivity and specificity values are 95.78% and 97.89%, respectively, indicating accurate detection of positive instances and low false positive rates. The precision is 96.00%, and the F1-score reaches 95.81%, reflecting a balanced performance between precision and recall. The false positive rate is 0.0211, representing minimal

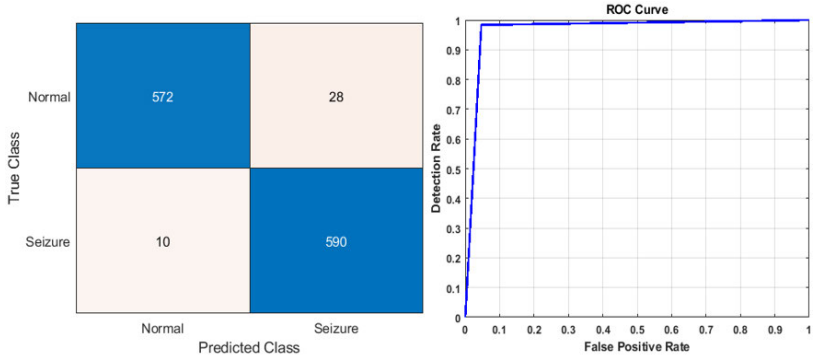

FIGURE 14. Confusion matrix and ROC curve for fully reconstructed EEG signal classification.

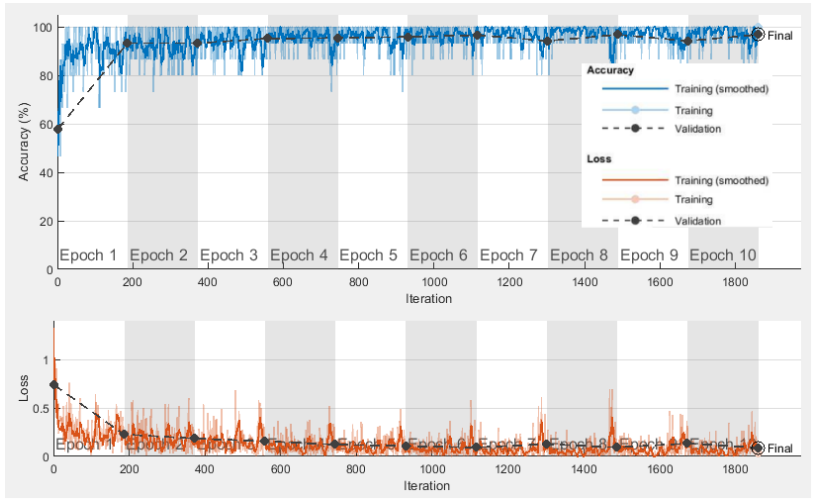

FIGURE 15. Training progress curve for the proposed CNN residual learning-based model with fully reconstructed EEG signal.

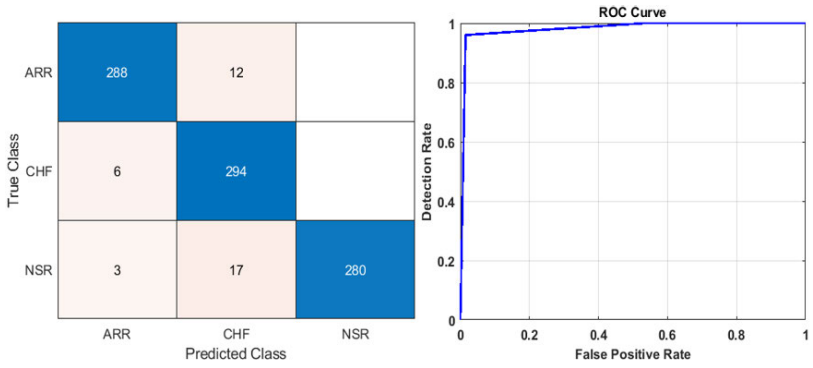

FIGURE 16. Confusion matrix and ROC curve for original EEG signal classification.

misclassification. In the CNN + compressed ECG scenario, the accuracy slightly decreases to 92.89% compared to the original ECG model, suggesting a minor impact from compression. However, sensitivity 92.89% and specificity 96.44% remain high, indicating effective ECG signal classification despite compression. Precision 93.78% and F1-score 92.99% values are also satisfactory. The false positive rate increases slightly to 0.0356. In the CNN + fully reconstructed ECG scenario, the accuracy achieves 94.89%, demonstrating competitive ECG classification performance. Sensitivity 94.89% and specificity 97.44% values are robust. Precision 95.03% and F1-score 94.91% also indicate accurate classification. The false positive rate is 0.0256. The CNN + original ECG model outperforms the other two, achieving the highest accuracy, sensitivity, specificity, precision, and F1-score. However, the CNN + compressed ECG and "CNN +

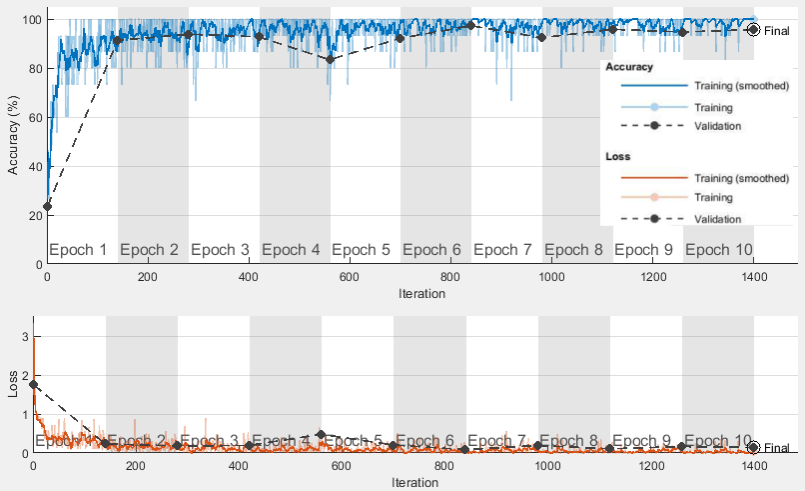

FIGURE 17. Training progress curve for the proposed CNN residual learning-based model with original EEG signal.

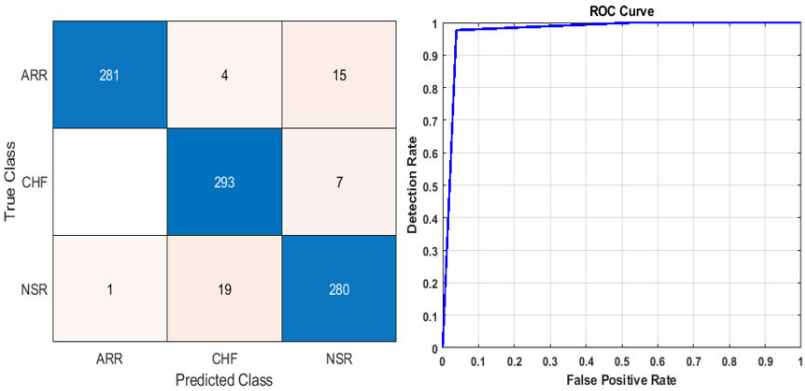

FIGURE 18. Confusion matrix and ROC curve for compressed EEG signal classification.

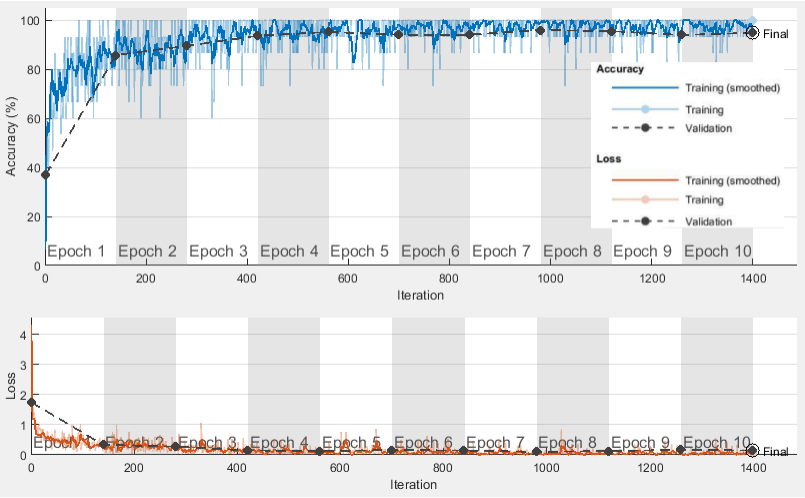

FIGURE 19. Training progress curve for the proposed CNN residual learning-based model with compressed EEG signal.

fully reconstructed ECG'' models display competitive performance, highlighting the potential of compressed and reconstructed ECG signals for efficient classification with reduced data size and without significant degradation in accuracy.

H. COMPREHENSIVE COMPARISON WITH RELATED STUDIES

Table 11 provides a comprehensive comparison of the proposed EEG classification system with several state-of-the-art methods, along with their corresponding performance

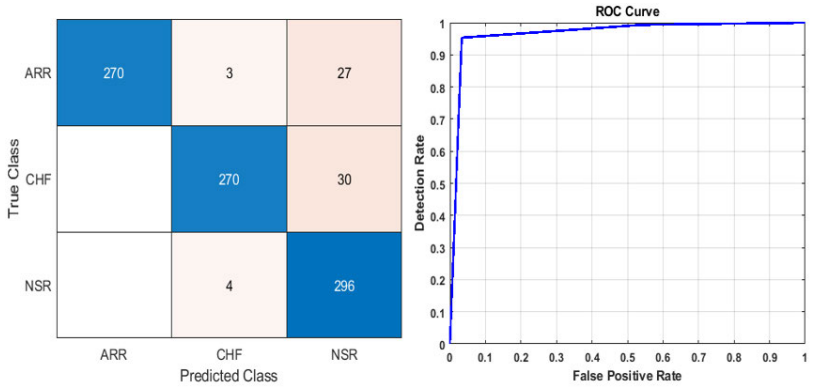

FIGURE 20. Confusion matrix and ROC curve for fully reconstructed EEG signal classification.

TABLE 11. Comparative analysis of the EEG classification system proposed in this study and other state-of-the-art systems.

Authors	Method	Performance metrics (%)		
		Acc	Sen	Spec
Li et al. [65]	Spectral, temporal, CE-stSENet	95.96	92.41	96.05
Yang et al. [66]	30 Statistical features + XGB	86.27	80.32	92.22
Hossain et al. [67]	Deep CNN, Dense + SoftMax	98.05	90.00	91.65
Khan et al. [68]	Statistical features, Change point detection	-	96.00	-
Li et al. [69]	EMD, DWT, CSP + multi-SVM fusion	97.49	97.34	97.50
Jiang et al. [70]	24 Statistical features + SVM	94.50	-	-
Tuauctan et al. [83]	SAE, Deep CNN, FC + SVM	92.00	95.00	90.00
Tang et al. [84]	Band energy & SVM	-	87.60	88.00
Zanetti et al. [71]	Statistical features &RF	-	96.60	92.50
Zabihi et al. [85]	LDA + ANN	95.11	91.15	95.16
Alkanhal et al. [86]	Deep CNN + SoftMax	-	87.95	86.50
Proposed Framwork	LBP+CNN+original EEG	97.33	99.17	95.50
	LBP+CNN+compressed EEG	96.50	99.00	94.00
	LBP+CNN+fully reconstructed EEG	96.83	95.33	98.33

metrics. Among the existing approaches, Li et al. [65] combined spectral, temporal, and CE-stSENet techniques, achieving an accuracy of 95.96%. Yang et al. [66] employed 30 statistical features with the XGBoost algorithm, yielding an accuracy of 86.27%. Hossain et al. [67] utilized a deep CNN with dense layers and softmax activation, achieving the highest accuracy of 98.05%. Khan et al. [68] focused on statistical features and change point detection, achieving a sensitivity of 96.00%. Li et al. [69] used EMD, DWT, and CSP combined with multi-SVM fusion, resulting in an accuracy of 97.49%. Jiang et al. [70] used 24 statistical features with SVM, achieving an accuracy of 94.50%. Tuauctan et al. [83] implemented an SAE, deep CNN, and FC layers with SVM, attaining a sensitivity of 95.00%. Tang et al. [84] focused on band energy features combined with SVM, achieving a specificity of 88.00%. Zanetti et al. [71] utilized statistical features with RF, resulting in a sensitivity of 96.60%. Zabihi et al. [85] employed LDA combined with ANN, achieving an accuracy of 95.11%. Alkanhal et al. [86] utilized a deep CNN with softmax activation, yielding a specificity of 86.50%. In comparison, the proposed framework using LBP+CNN with original EEG data achieves an impressive accuracy of 97.33%. This outperforms most of the existing methods. Furthermore, the

TABLE 12. Comparative analysis of the ECG multi-class classification system proposed in this study and other state-of-the-art systems.

Authors	Subjects from MIT-BIH NSR, MIT-BIH ARR, and	Approach	Performance (%)		
			Sen	Spec	Acc
Cornforth et al. [42]	BIDMC CHF Databases 18 NSR 15 CHF	Renyi entropy combined with conventional HRV features using K-NN classifier	80.0	94.4	87.9
Chen et al. [43]	54 NSR RR 18 NSR 29 CHF RR 15 CHF	Multistage CHF detection system using short-term HRV dynamic measures and decision-tree-based SVM classifier	95.39	100	96.91
Kumar et al. [44]	18 NSR 15 CHF	HRV fuzzy and permutation entropies at different frequency scales with the least squares SVM classifier	98.07	98.33	98.21
Wang et al. [45]	52 NSR RR 18 CHF RR	ECG handcrafted features with SVM classifier	91.31	90.04	90.95
Hu et al. [46]	54 NSR RR 29 CHF RR	Multiple time scales HRV analysis with SVM classifier	93.33	98.33	94.44
Li et al. [47]	54 NSR ARR 29 CHF RR	Pre-trained CNN combined with distance distribution matrix in entropy calculation	80.99	–	81.34
Kaouter et al. [50]	18 NSR 15 CHF 47 ARR	CNN with CWT algorithm	–	–	93.75
Acharya et al. [48]	18 NSR 15 CHF	11-layer deep CNN for CHF diagnosis	96.52	95.75	95.98
Wang et al. [49]	54 NSR RR 29 CHF RR	Short-term HRV analysis and deep CNN	76.71	99.22	87.54
Ccinar et al. [51]	18 NSR 15 CHF 47 ARR	Hybrid AlexNet-SVM deep neural networks and STFT	95.00	–	96.77
Kumari et al. [52]	18 NSR 15 CHF 47 ARR	DWT features with SVM classifier	92.59	–	95.92
Kumari et al. [53]	18 NSR 15 CHF 47 ARR	Feature extraction using CWT algorithm and classification with SVM	92.59	–	95.92
Eltrass et al. [54]	18 NSR 15 CHF 47 ARR	Hybrid deep CNN approach combined with HRV and ECG features using PTWF feature selection algorithm and LDA classifier	98.17	99.00	98.74
Proposed Framework	36 NSR 30 CHF 96 ARR	LBP+CNN+ original ECG	95.78	97.89	95.78
		LBP+CNN+ compressed ECG	92.89	96.44	92.89
		LBP+CNN+ fully reconstructed ECG	94.89	97.44	94.89

system exhibits a high sensitivity of 99.17%, indicating its excellent ability to detect seizure activity, and a specificity of 95.50%, reflecting its proficiency in identifying normal brain activity. The performance of the proposed framework remains consistently high when using compressed and fully reconstructed EEG data, indicating its robustness. Overall, the results highlight the superiority of the proposed EEG classification system over the state-of-the-art methods listed in the table. The high accuracy and sensitivity suggest the potential of the proposed framework for accurate and reliable seizure detection in EEG signals.

Table 12 compares various methods for ECG classification. Our proposed framework outperforms several existing systems [42], [43], [44], [45], [46], [47], [48], [49] in distinguishing between patients with CHF and NSR. Using original ECG signals, our approach achieves a sensitivity of 95.78% and specificity of 97.89%, surpassing the results of previous studies [42], [43], [44], [45], [45], [46], [47], [50]. Moreover, our framework consistently performs well with compressed and fully reconstructed ECG signals, achieving sensitivities of 92.89% and 94.89%, and specificities of 96.44% and 97.44%, respectively. These results demonstrate

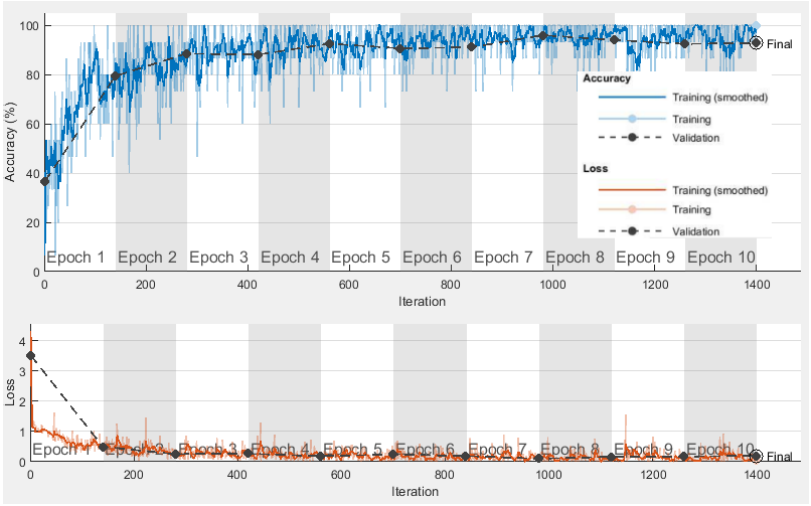

FIGURE 21. Training progress curve for the proposed CNN residual learning-based model with fully reconstructed EEG signal.

the effectiveness and versatility of our approach in accurately classifying ECG signals, regardless of their compression level. Overall, our framework exhibits superior performance in CHF and NSR classification, indicating its potential for improved cardiac disease diagnosis and patient care.

V. CONCLUSION

This paper has presented a comprehensive approach for the efficient compression and classification of EEG and ECG signals in WBAN systems. The proposed methodology addresses key challenges in signal representation, noise interference, and computational complexity, offering promising solutions for real-time monitoring and diagnosis in healthcare systems. The sequential approach introduced in this study incorporates the optimized Walsh-Hadamard transform (OWHT) for signal compression, the SPGL1 algorithm for signal recovery, and a local binary pattern (LBP) approach for feature extraction. The evaluation of the proposed algorithm demonstrated its effectiveness in accurately reconstructing the signals while mitigating the impact of noise interference. The results indicated a significant reduction in MSE values compared to other compression techniques, highlighting the superior performance of the proposed method. The integration of a classification algorithm based on residual learning enables high-accuracy classification of the compressed EEG and ECG signals without the need for signal recovery. The evaluation of the classification performance demonstrates the effectiveness of the proposed algorithm. For instance, the classification accuracy achieved for the compressed ECG signals was 92.89%, outperforming other methods. This showcases the potential of the proposed approach in achieving accurate and reliable classification results. However, there are certain limitations to this study that should be acknowledged. Firstly, the proposed methodology focuses specifically on EEG and ECG signals and may not be directly applicable to other types of medical signals. Further research is needed to adapt and validate the approach for other modalities. Secondly, the performance evaluation of the algorithm was conducted on specific datasets and under controlled conditions. Extending the evaluation to diverse datasets and real-world scenarios would provide a more comprehensive assessment of its robustness and generalizability. Future work should aim to address these limitations and explore additional avenues for improvement. One potential direction is to investigate the scalability and efficiency of the proposed methodology in large-scale WBAN systems with multiple nodes. Additionally, incorporating advanced machine learning techniques and deep learning models could further enhance classification accuracy and enable the detection of more complex medical conditions. Moreover, conducting user studies to evaluate the proposed approach in real-world settings and comparing it with existing methods would provide valuable insights into its practical utility and performance.

REFERENCES

[1] D. Needell and J. A. Tropp, "CoSaMP: Iterative signal recovery from incomplete and inaccurate samples," *Commun. ACM*, vol. 53, no. 12, pp. 93–100, Dec. 2010.

[2] J. Chen, S. Sun, L.-B. Zhang, B. Yang, and W. Wang, "Compressed sensing framework for heart sound acquisition in Internet of Medical Things," *IEEE Trans. Ind. Informat.*, vol. 18, no. 3, pp. 2000–2009, Mar. 2022.

[3] O. Pereira, J. M. L. P. Caldeira, and J. J. P. C. Rodrigues, "Body sensor network mobile solutions for biofeedback monitoring," *Mobile Netw. Appl.*, vol. 16, no. 6, pp. 713–732, Dec. 2011.

[4] J. Chen, S. Sun, N. Bao, Z. Zhu, and L.-B. Zhang, "Improved reconstruction for CS-based ECG acquisition in Internet of Medical Things," *IEEE Sensors J.*, vol. 21, no. 22, pp. 25222–25233, Nov. 2021.

[5] R. Cavallari, F. Martelli, R. Rosini, C. Buratti, and R. Verdone, "A survey on wireless body area networks: Technologies and design challenges," *IEEE Commun. Surveys Tuts.*, vol. 16, no. 3, pp. 1635–1657, 3rd Quart., 2014.

[6] Z. Zhang, T.-P. Jung, S. Makeig, and B. D. Rao, "Compressed sensing of EEG for wireless telemonitoring with low energy consumption and inexpensive hardware," *IEEE Trans. Biomed. Eng.*, vol. 60, no. 1, pp. 221–224, Jan. 2013.

[7] Z. Zhang, T.-P. Jung, S. Makeig, Z. Pi, and B. D. Rao, "Spatiotemporal sparse Bayesian learning with applications to compressed sensing of multichannel physiological signals," *IEEE Trans. Neural Syst. Rehabil. Eng.*, vol. 22, no. 6, pp. 1186–1197, Nov. 2014.

[8] H.-J. Yoo and J. Bae, "Low energy wireless body area network systems," in *Proc. IEEE Int. Wireless Symp. (IWS)*, Apr. 2013, pp. 1–2.

[9] M. Blanco-Velasco, F. Cruz-Roldán, J. I. Godino-Llorente, J. Blanco-Velasco, C. Armiens-Aparicio, and F. López-Ferreras, "On the use of PRD and CR parameters for ECG compression," *Med. Eng. Phys.*, vol. 27, no. 9, pp. 798–802, Nov. 2005.

[10] M. Babakmehr, M. G. Simoes, M. B. Wakin, and F. Harirchi, "Compressive sensing-based topology identification for smart grids," *IEEE Trans. Ind. Informat.*, vol. 12, no. 2, pp. 532–543, Apr. 2016.

[11] Y. Gao and Y. Wu, "Recent advances of chitosan-based nanoparticles for biomedical and biotechnological applications," *Int. J. Biol. Macromolecules*, vol. 203, pp. 379–388, Apr. 2022.

[12] A. N. Bahache, N. Chikouche, and F. Mezrag, "Authentication schemes for healthcare applications using wireless medical sensor networks: A survey," *Social Netw. Comput. Sci.*, vol. 3, no. 5, p. 382, Jul. 2022.

[13] N. V. L. M. K. Munagala, A. D. Rani, and D. V. R. K. Reddy, "Blockchain-based Internet-of-Things for secure transmission of medical data in rural areas," *Comput. J.*, vol. 5, Aug. 2022, Art. no. bxac113.

[14] L.-B. Zhang, S. Sun, J. Chen, Y. Teng, and Z. Lv, "Self-adaptive reconstruction for compressed sensing based ECG acquisition in wireless body area network," *Future Gener. Comput. Syst.*, vol. 142, pp. 228–236, May 2023.

[15] Z. Loring, S. Sen, E. Black-Maier, B. D. Atwater, S. D. Russell, A. D. DeVore, and J. P. Piccini, "Reducing ECG artifact from left ventricular assist device electromagnetic interference," *J. Amer. Heart Assoc.*, vol. 9, no. 16, Aug. 2020, Art. no. e017563.

[16] P. Zhou, B. Lock, and T. A. Kuiken, "Real time ECG artifact removal for myoelectric prosthesis control," *Physiological Meas.*, vol. 28, no. 4, pp. 397–413, Apr. 2007.

[17] G. G. Berntson and J. R. Stowell, "ECG artifacts and heart period variability: Don't miss a beat!" *Psychophysiology*, vol. 35, no. 1, pp. 127–132, Jan. 1998.

[18] H. M. Emara, M. R. Shoaib, M. Elwekeil, W. El-Shafai, T. E. Taha, A. S. El-Fishawy, E.-S. M. El-Rabaie, S. A. Alshebeili, M. I. Dessouky, and F. E. A. El-Samie, "Deep convolutional neural networks for COVID-19 automatic diagnosis," *Microsc. Res. Technique*, vol. 84, no. 11, pp. 2504–2516, 2021.

[19] A. Sedik, H. M. Emara, A. Hamad, E. M. Shahin, N. A. El-Hag, A. Khalil, F. Ibrahim, Z. M. Elsherbeny, M. Elreefy, and O. Zahran, "Efficient anomaly detection from medical signals and images," *Int. J. Speech Technol.*, vol. 22, pp. 739–767, Sep. 2019.

[20] F. M. Ghamry, H. M. Emara, A. Hagag, W. El-Shafai, G. M. El-Banby, M. I. Dessouky, A. S. El-Fishawy, N. A. El-Hag, and F. E. A. El-Samie, "Efficient algorithms for compression and classification of brain tumor images," *J. Opt.*, vol. 52, no. 2, pp. 818–830, 2023.

[21] F. Taher, M. R. Shoaib, H. M. Emara, K. M. Abdelwahab, F. E. A. El-Samie, and M. T. Haweel, "Efficient framework for brain tumor detection using different deep learning techniques," *Frontiers Public Health*, vol. 10, Dec. 2022, Art. no. 959667.

[22] H. M. Emara, M. R. Shoaib, W. El-Shafai, M. Elwekeil, E. E.-D. Hemdan, M. M. Fouda, T. E. Taha, A. S. El-Fishawy, E.-S.-M. El-Rabaie, and F. E. A. El-Samie, "Simultaneous super-resolution and classification of lung disease scans," *Diagnostics*, vol. 13, no. 7, p. 1319, Apr. 2023.

[23] M. R. Shoaib, H. M. Emara, M. Elwekeil, W. El-Shafai, T. E. Taha, A. S. El-Fishawy, E.-S.-M. El-Rabaie, and F. E. A. El-Samie, "Hybrid classification structures for automatic COVID-19 detection," *J. Ambient Intell. Humanized Comput.*, vol. 13, no. 9, pp. 4477–4492, Sep. 2022.

[24] M. R. Shoaib, M. R. Elshamy, T. E. Taha, A. S. El-Fishawy, and F. E. A. El-Samie, "Efficient deep learning models for brain tumor detection with segmentation and data augmentation techniques," *Concurrency Comput., Pract. Exper.*, vol. 34, no. 21, p. e7031, Sep. 2022.

[25] M. R. Shoaib, M. R. Elshamy, T. E. Taha, A. S. El-Fishawy, and F. E. A. El-Samie, "Efficient brain tumor detection based on deep learning models," *J. Phys., Conf.*, vol. 2128, no. 1, Dec. 2021, Art. no. 012012.

[26] M. H. Aghababaei, G. Azemi, and J. M. O'Toole, "Detection of epileptic seizures from compressively sensed EEG signals for wireless body area networks," *Exp. Syst. Appl.*, vol. 172, Jun. 2021, Art. no. 114630.

[27] D. Bhati, A. Raikwar, R. B. Pachori, and V. M. Gadre, "Three channel wavelet filter banks with minimal time frequency spread for classification of seizure-free and seizure EEG signals," in *Handbook of Research on Advancements of Artificial Intelligence in Healthcare Engineering*. IGI Global, 2020, pp. 220–236.

[28] A. Bhattacharyya and R. B. Pachori, "A multivariate approach for patient-specific EEG seizure detection using empirical wavelet transform," *IEEE Trans. Biomed. Eng.*, vol. 64, no. 9, pp. 2003–2015, Sep. 2017.

[29] D. Bhati, R. B. Pachori, M. Sharma, and V. M. Gadre, "Automated detection of seizure and nonseizure EEG signals using two band biorthogonal wavelet filter banks," in *Biomedical Signal Processing: Advances in Theory, Algorithms and Applications*. Berlin, Germany: Springer, 2019, pp. 137–155.

[30] M. T. Sadiq, X. Yu, Z. Yuan, M. Z. Aziz, S. Siuly, and W. Ding, "A matrix determinant feature extraction approach for decoding motor and mental imagery EEG in subject-specific tasks," *IEEE Trans. Cognit. Develop. Syst.*, vol. 14, no. 2, pp. 375–387, Jun. 2022.

[31] B. B. Borah, U. Hazarika, S. M. B. Baruah, S. Roy, and A. Jamir, "A BCI framework for smart home automation using EEG signal," *Intell. Decis. Technol.*, pp. 1–19, 2023.

[32] K. Zeng, J. Yan, Y. Wang, A. Sik, G. Ouyang, and X. Li, "Automatic detection of absence seizures with compressive sensing EEG," *Neurocomputing*, vol. 171, pp. 497–502, Jan. 2016.

[33] V. S. Unni, R. G. Gavaskar, and K. N. Chaudhury, "Compressive sensing of ECG signals using plug-and-play regularization," *Signal Process.*, vol. 202, Jan. 2023, Art. no. 108738.

[34] G. Rosa, M. Russodivito, G. Laudato, A. R. Colavita, L. D. Vito, F. Picariello, S. Scalabrino, I. Tudosa, and R. Oliveto, "Multi-class detection of arrhythmia conditions through the combination of compressed sensing and machine learning," in *Biomedical Engineering Systems and Technologies*. Berlin, Germany: Springer, 2023, pp. 213–235.

[35] S. Kumar, S. Prasad, and B. Lall, "A compressive sensing codec architecture for ECG signals with adaptive quantization and stream entropy coding," Indian Inst. Technol., India, Tech. Rep. 2, 2023.

[36] M. Fira, H.-N. Costin, and L. Goraş, "A study on dictionary selection in compressive sensing for ECG signals compression and classification," *Biosensors*, vol. 12, no. 3, p. 146, Feb. 2022.

[37] R. Aghazadeh, J. Frounchi, F. Montagna, and S. Benatti, "Scalable and energy efficient seizure detection based on direct use of compressively-sensed EEG data on an ultra low power multi-core architecture," *Comput. Biol. Med.*, vol. 125, Oct. 2020, Art. no. 104004.

[38] J. Hua, J. Rao, Y. Peng, J. Liu, and J. Tang, "Deep compressive sensing on ECG signals with modified inception block and LSTM," *Entropy*, vol. 24, no. 8, p. 1024, Jul. 2022.

[39] K.-S. Lee, H.-J. Park, J. E. Kim, H. J. Kim, S. Chon, S. Kim, J. Jang, J.-K. Kim, S. Jang, Y. Gil, and H. S. Son, "Compressed deep learning to classify arrhythmia in an embedded wearable device," *Sensors*, vol. 22, no. 5, p. 1776, Feb. 2022.

[40] M. Abdelazez, S. Rajan, and A. D. C. Chan, "Signal quality assessment of compressively sensed electrocardiogram," *IEEE Trans. Biomed. Eng.*, vol. 69, no. 11, pp. 3397–3406, Nov. 2022.

[41] H. Zhang, Z. Dong, Z. Wang, L. Guo, and Z. Wang, "CSNet: A deep learning approach for ECG compressed sensing," *Biomed. Signal Process. Control*, vol. 70, Sep. 2021, Art. no. 103065.

[42] D. J. Cornforth and H. F. Jelinek, "Detection of congestive heart failure using Renyi entropy," in *Proc. Comput. Cardiology Conf. (CinC)*, Sep. 2016, pp. 669–672.

[43] W. Chen, L. Zheng, K. Li, Q. Wang, G. Liu, and Q. Jiang, "A novel and effective method for congestive heart failure detection and quantification using dynamic heart rate variability measurement," *PLoS ONE*, vol. 11, no. 11, Nov. 2016, Art. no. e0165304.

[44] M. Kumar, R. Pachori, and U. Acharya, "Use of accumulated entropies for automated detection of congestive heart failure in flexible analytic wavelet transform framework based on short-term HRV signals," *Entropy*, vol. 19, no. 3, p. 92, Feb. 2017.

[45] Y. Wang, S. Wei, S. Zhang, Y. Zhang, L. Zhao, C. Liu, and A. Murray, "Comparison of time-domain, frequency-domain and non-linear analysis for distinguishing congestive heart failure patients from normal sinus rhythm subjects," *Biomed. Signal Process. Control*, vol. 42, pp. 30–36, Apr. 2018.

[46] B. Hu, S. Wei, D. Wei, L. Zhao, G. Zhu, and C. Liu, "Multiple time scales analysis for identifying congestive heart failure based on heart rate variability," *IEEE Access*, vol. 7, pp. 17862–17871, 2019.

[47] Y. Li, Y. Zhang, L. Zhao, Y. Zhang, C. Liu, L. Zhang, L. Zhang, Z. Li, B. Wang, E. Ng, J. Li, and Z. He, "Combining convolutional neural network and distance distribution matrix for identification of congestive heart failure," *IEEE Access*, vol. 6, pp. 39734–39744, 2018.

[48] U. R. Acharya, H. Fujita, S. L. Oh, Y. Hagiwara, J. H. Tan, M. Adam, and R. S. Tan, "Deep convolutional neural network for the automated diagnosis of congestive heart failure using ECG signals," *Int. J. Speech Technol.*, vol. 49, no. 1, pp. 16–27, Jan. 2019.

[49] L. Wang, W. Zhou, Q. Chang, J. Chen, and X. Zhou, "Deep ensemble detection of congestive heart failure using short-term RR intervals," *IEEE Access*, vol. 7, pp. 69559–69574, 2019.

[50] K. Kaouter, T. Mohamed, D. Sofiene, D. Abbas, and M. Fouad, "Full training convolutional neural network for ecg signals classification," in *Proc. AIP Conf.*, vol. 2190, 2019, Art. no. 020055.

[51] A. Cínar and S. A. Tuncer, "Classification of normal sinus rhythm, abnormal arrhythmia and congestive heart failure ecg signals using LSTM and hybrid CNN-SVM deep neural networks," *Comput. Methods Biomechanics Biomed. Eng.*, vol. 24, no. 2, pp. 203–214, 2021.

[52] C. U. Kumari, A. S. D. Murthy, B. L. Prasanna, M. P. P. Reddy, and A. K. Panigrahy, "An automated detection of heart arrhythmias using machine learning technique: SVM," *Mater. Today, Proc.*, vol. 45, pp. 1393–1398, Jan. 2021.

[53] Ch. U. Kumari, R. Ankita, T. Pavani, N. A. Vignesh, N. T. Varma, M. A. Manzar, and A. Reethika, "Heart rhythm abnormality detection and classification using machine learning technique," in *Proc. 4th Int. Conf. Trends Electron. Informat. (ICOEI)*, Jun. 2020, pp. 580–584.

[54] A. S. Eltrass, M. B. Tayel, and A. I. Ammar, "Automated ECG multi-class classification system based on combining deep learning features with HRV and ECG measures," *Neural Comput. Appl.*, vol. 34, no. 11, pp. 8755–8775, Jun. 2022.

[55] S. M. Qaisar, "Adaptive rate EEG processing and machine learning-based efficient recognition of epilepsy," in *Advanced Methods in Biomedical Signal Processing and Analysis*. Amsterdam, The Netherlands: Elsevier, 2023, pp. 341–373.

[56] M. Rani, S. Dhok, and R. Deshmukh, "Compressive sensing-based continuous EEG monitoring: Seizure detection performance comparison of different classifiers," in *Advances in VLSI, Communication, and Signal Processing*. Berlin, Germany: Springer, 2021, pp. 459–468.

[57] Y. Liu, M. De Vos, and S. Van Huffel, "Compressed sensing of multichannel EEG signals: The simultaneous cosparsity and low-rank optimization," *IEEE Trans. Biomed. Eng.*, vol. 62, no. 8, pp. 2055–2061, Aug. 2015.

[58] L. T. Tan and L. B. Le, "Joint data compression and MAC protocol design for smartgrids with renewable energy," *Wireless Commun. Mobile Comput.*, vol. 16, no. 16, pp. 2590–2604, Nov. 2016.

[59] Q. Wan, H. Duan, J. Fang, H. Li, and Z. Xing, "Robust Bayesian compressed sensing with outliers," *Signal Process.*, vol. 140, pp. 104–109, Nov. 2017.

[60] C. Li, W. Tao, J. Cheng, Y. Liu, and X. Chen, "Robust multichannel EEG compressed sensing in the presence of mixed noise," *IEEE Sensors J.*, vol. 19, no. 22, pp. 10574–10583, Nov. 2019.

[61] M. Rani, S. Dhok, and R. Deshmukh, "EEG seizure detection from compressive measurements," in *Advances in VLSI, Communication, and Signal Processing*. Berlin, Germany: Springer, 2020, pp. 963–969.

[62] R. Kunabeva, L. Vinutha, and P. Manjunatha, "In-node adaptive compressive sensing technique for EEG signal in WBAN," in *Data Intelligence and Cognitive Informatics*. Berlin, Germany: Springer, 2022, pp. 705–719.

[63] S. Sheykhivand, T. Y. Rezaii, S. Meshgini, S. Makoui, and A. Farzamnia, "Developing a deep neural network for driver fatigue detection using EEG signals based on compressed sensing," *Sustainability*, vol. 14, no. 5, p. 2941, Mar. 2022.

[64] J. Van Assche, R. Helsen, and G. Gielen, "EffiCSense: An architectural pathfinding framework for energy-constrained sensor applications," in *Proc. Design, Autom. Test Eur. Conf. Exhib. (DATE)*, Mar. 2022, pp. 136–141.

[65] Y. Li, Y. Liu, W.-G. Cui, Y.-Z. Guo, H. Huang, and Z.-Y. Hu, "Epileptic seizure detection in EEG signals using a unified temporal-spectral squeeze-and-excitation network," *IEEE Trans. Neural Syst. Rehabil. Eng.*, vol. 28, no. 4, pp. 782–794, Apr. 2020.

[66] S. Yang, B. Li, Y. Zhang, M. Duan, S. Liu, Y. Zhang, X. Feng, R. Tan, L. Huang, and F. Zhou, "Selection of features for patient-independent detection of seizure events using scalp EEG signals," *Comput. Biol. Med.*, vol. 119, Apr. 2020, Art. no. 103671.

[67] M. S. Hossain, S. U. Amin, M. Alsulaiman, and G. Muhammad, "Applying deep learning for epilepsy seizure detection and brain mapping visualization," *ACM Trans. Multimedia Comput., Commun., Appl.*, vol. 15, no. 1s, pp. 1–17, Jan. 2019.

[68] S. Khanmohammadi and C.-A. Chou, "Adaptive seizure onset detection framework using a hybrid PCA–CSP approach," *IEEE J. Biomed. Health Informat.*, vol. 22, no. 1, pp. 154–160, Jan. 2018.

[69] C. Li, W. Zhou, G. Liu, Y. Zhang, M. Geng, Z. Liu, S. Wang, and W. Shang, "Seizure onset detection using empirical mode decomposition and common spatial pattern," *IEEE Trans. Neural Syst. Rehabil. Eng.*, vol. 29, pp. 458–467, 2021.

[70] Z. Jiang and W. Zhao, "Optimal selection of customized features for implementing seizure detection in wearable electroencephalography sensor," *IEEE Sensors J.*, vol. 20, no. 21, pp. 12941–12949, Nov. 2020.

[71] R. Zanetti, A. Aminifar, and D. Atienza, "Robust epileptic seizure detection on wearable systems with reduced false-alarm rate," in *Proc. 42nd Annu. Int. Conf. IEEE Eng. Med. Biol. Soc. (EMBC)*, Jul. 2020, pp. 4248–4251.

[72] J. Prasanna, M. S. P. Subathra, M. A. Mohammed, R. Damaševičius, N. J. Sairamya, and S. T. George, "Automated epileptic seizure detection in pediatric subjects of CHB-MIT EEG database—A survey," *J. Personalized Med.*, vol. 11, no. 10, p. 1028, Oct. 2021.

[73] A. L. Goldberger, L. A. N. Amaral, L. Glass, J. M. Hausdorff, P. C. Ivanov, R. G. Mark, J. E. Mietus, G. B. Moody, C.-K. Peng, and H. E. Stanley, "PhysioBank, PhysioToolkit, and PhysioNet: Components of a new research resource for complex physiologic signals," *Circulation*, vol. 101, no. 23, pp. 215–220, Jun. 2000.

[74] G. B. Moody and R. G. Mark, "The impact of the MIT-BIH arrhythmia database," *IEEE Eng. Med. Biol. Mag.*, vol. 20, no. 3, pp. 45–50, 2001.

[75] D. S. Baim, W. S. Colucci, E. S. Monrad, H. S. Smith, R. F. Wright, A. Lanoue, D. F. Gauthier, B. J. Ransil, W. Grossman, and E. Braunwald, "Survival of patients with severe congestive heart failure treated with oral milrinone," *J. Amer. College Cardiol.*, vol. 7, no. 3, pp. 661–670, Mar. 1986.

[76] M. Davenport, "The fundamentals of compressive sensing," *IEEE Signal Process. Soc. Online Tutorial Library*, vol. 3, no. 5, pp. 12–61, Feb. 2023.

[77] J. Dauwels, K. Srinivasan, M. R. Reddy, and A. Cichocki, "Near-lossless multichannel EEG compression based on matrix and tensor decompositions," *IEEE J. Biomed. Health Informat.*, vol. 17, no. 3, pp. 708–714, May 2013.

[78] M. Wang, Q. Wang, D. Hong, S. K. Roy, and J. Chanussot, "Learning tensor low-rank representation for hyperspectral anomaly detection," *IEEE Trans. Cybern.*, vol. 53, no. 1, pp. 679–691, Jan. 2023.

[79] V. Gupta, A. Bhattacharyya, and R. B. Pachori, "Automated identification of epileptic seizures from EEG signals using FBSE-EWT method," in *Biomedical Signal Processing*. Singapore: Springer, 2020, pp. 157–179.

[80] A. A. Rahimi, H. Hu, K. Sivakumar, and S. Gupta, "Energy-efficient serialized Walsh-Hadamard transform based feature-extraction for information-aware compressive sensing," in *Proc. IEEE Int. Symp. Circuits Syst. (ISCAS)*, May 2018, pp. 1–5.

[81] K. Markham. (2020). *Simple Guide to Confusion Matrix Terminology 2014*. [Online]. Available: http://www.dataschool.io/simple-guide-to-confusion-matrix-terminology

[82] D. M. W. Powers, "Evaluation: From precision, recall and F-measure to ROC, informedness, markedness and correlation," 2020, *arXiv:2010.16061*.

[83] A.-M. Tautan, M. Dogariu, and B. Ionescu, "Detection of epileptic seizures using unsupervised learning techniques for feature extraction," in *Proc. 41st Annu. Int. Conf. IEEE Eng. Med. Biol. Soc. (EMBC)*, Jul. 2019, pp. 2377–2381.

[84] Z. Tang, C. Zhang, Y. Song, and M. Zhang, "Design of a seizure detector using single channel EEG signal," in *Proc. IEEE Int. Symp. Circuits Syst. (ISCAS)*, May 2021, pp. 1–4.

[85] M. Zabihi, S. Kiranyaz, V. Jäntti, T. Lipping, and M. Gabbouj, "Patient-specific seizure detection using nonlinear dynamics and nullclines," *IEEE J. Biomed. Health Informat.*, vol. 24, no. 2, pp. 543–555, Feb. 2020.

[86] I. Alkanhal, B. V. K. V. Kumar, and M. Savvides, "Automatic seizure detection via an optimized image-based deep feature learning," in *Proc. 17th IEEE Int. Conf. Mach. Learn. Appl. (ICMLA)*, Dec. 2018, pp. 536–540.

HEBA M. EMARA received the B.Sc., M.Sc., and Ph.D. degrees from the Faculty of Electronic Engineering, Menoufia University, Menouf, Egypt, in 2002, 2019, and 2022, respectively. She is currently a Lecturer and an Assistant Professor with the Electronics and Communication Engineering (ECE) Department, Department of Electronics and Communications Engineering, Pyramids High Institute of Electronic Engineering, Ministry of Higher Education, 6th of October, Giza, Egypt. Her research interests include image and signal processing, medical image processing, security algorithms, medical diagnoses applications, artificial intelligence for signal processing algorithms and communication systems, modulation identification and classification, deep learning in signal processing, and communication systems applications. She has several publications in the above research areas in several reputable international and local journals. Also, she serves as a reviewer for several international journals.

WALID EL-SHAFAI (Senior Member, IEEE) was born in Alexandria, Egypt. He received the B.Sc. degree (Hons.) in electronics and electrical communication engineering from the Faculty of Electronic Engineering (FEE), Menoufia University, Menouf, Egypt, in 2008, the M.Sc. degree from the Egypt-Japan University of Science and Technology (E-JUST), in 2012, and the Ph.D. degree from the Faculty of Electronic Engineering, Menoufia University, in 2019. Since January 2021, he has been a Postdoctoral Research Fellow with the Security Engineering Laboratory (SEL), Prince Sultan University (PSU), Riyadh, Saudi Arabia. He is currently a Lecturer and an Assistant Professor with the Electronics and Communication Engineering (ECE) Department, FEE, Menoufia University. His research interests include wireless mobile and multimedia communications systems, image and video signal processing, efficient 2D video/3D multi-view video coding, multi-view video plus depth coding, 3D multi-view video coding and transmission, the quality of service and experience, digital communication techniques, cognitive radio networks, adaptive filters design, 3D video watermarking, steganography, and encryption, error resilience and concealment algorithms for H.264/AVC, H.264/MVC, and H.265/HEVC video codecs standards, cognitive cryptography, medical image processing, speech processing, security algorithms, software defined networks, the Internet of Things, medical diagnoses applications, FPGA implementations for signal processing algorithms and communication systems, cancellable biometrics and pattern recognition, image and video magnification, artificial intelligence for signal processing algorithms and communication systems, modulation identification and classification, image and video super-resolution and denoising, cybersecurity applications, malware and ransomware detection and analysis, deep learning in signal processing, and communication systems applications. He has several publications in the above research areas in several reputable international and local journals and conferences. Also, he serves as a reviewer for several international journals.

ABEER D. ALGARNI received the B.Sc. degree (Hons.) in computer science from King Saud University, Riyadh, Saudi Arabia, in 2007, and the M.Sc. and Ph.D. degrees from the School of Engineering and Computer Sciences, Durham University, U.K., in 2010 and 2015, respectively. She has been an Assistant Professor with the College of Computer and Information Sciences, Princess Nourah Bint Abdulrahman University, since 2008. Her current research interests include networking and communication systems, digital image processing, digital communications, and cyber security.

NAGLAA F. SOLIMAN received the B.Sc., M.Sc., and Ph.D. degrees from the Faculty of Engineering, Zagazig University, Egypt, in 1999, 2004, and 2011, respectively. She was with the Faculty of Computer Science, Princess Nourah Bint Abdulrahman University, Saudi Arabia. Since 2015, she has been a Teaching Staff Member with the Department of Electronics and Communications Engineering, Faculty of Engineering, Zagazig University, Egypt. Her current research interests include digital image processing, information security, multimedia communications, medical image processing, optical signal processing, big data, and cloud computing.

FATHI E. ABD EL-SAMIE received the B.Sc. (Hons.), M.Sc., and Ph.D. degrees from the Faculty of Electronic Engineering, Menoufia University, Menouf, Egypt, in 1998, 2001, and 2005, respectively. He joined as a Teaching Staff of the Department of Electronics and Electrical Communications, Faculty of Electronic Engineering, Menoufia University, in 2005. He received the most cited paper award from *Digital Signal Processing* journal, in 2008. His current research interests include image enhancement, image restoration, image interpolation, the super-resolution reconstruction of images, data hiding, multimedia communications, medical image processing, optical signal processing, and digital communications.